

CHAPTER-2

LITERATURE REVIEW



2.1 Corrosion of Metals & alloys

2.1.1 Definitions of corrosion:

Corrosion of metal could be considered as reverse of extractive metallurgy. Extractive metallurgy concerned primarily with the winning of the metal from the ore and refining or alloying the metal for the use that may lead to considerable increase in the free energy. So the finished product reacts chemically or electrochemically with its surrounding environment to release the energy. Hence, it is defined as the destruction metal or deterioration of material physical properties due to chemical or electrochemical reactions with its surrounding environment [5].

2.1.2 Types of corrosion:

Fontana and Greene had categorized corrosion in eight form based on visual characteristics of the morphology of attack. These forms are uniform attack, crevice corrosion, pitting, inter-granular corrosion, selective leaching, erosion corrosion, stress corrosion, and hydrogen damage. Substantial advances in the field of corrosion science have begun to define the mechanisms of many forms of corrosion more clearly. The forms of corrosion were categorized to represent the mechanisms of attack involved rather than to emphasize the visual characteristics as follows.

2.1.3. Forms of corrosion:

2.1.3.1 General corrosion

- Atmospheric corrosion
- Galvanic corrosion
- Stray-current corrosion
- General biological corrosion
- Molten salt corrosion
- Corrosion in liquid metals
- High-temperature corrosion
- Oxidation
- Sulfidation
- Carburization
- Other forms(a)

2.1.3.2 Localized corrosion

- Filiform corrosion
- Crevice corrosion
- Pitting corrosion
- Localized biological corrosion

2.1.3.3 Metallurgically influenced corrosion

- Intergranular corrosion
- Dealloying corrosion

2.1.3.4 Mechanically assisted degradation

- Erosion corrosion
- Fretting corrosion
- Cavitation and water drop impingement
- Corrosion fatigue

2.1.3.5 Environmentally induced cracking

- Stress-corrosion cracking
- Hydrogen damage
- Liquid metal embrittlement
- Solid metal induced embrittlement

2.1.4 Corrosion Prevention method:**2.1.4.1 Material Selection:**

The most common method of preventing corrosion is the selection of the proper metal or alloy for a particular corrosive service. In alloy selection, there are several “natural” metal-corrosive combinations which usually represent the maximum amount of corrosion resistance for the least amount of money. Some of natural combinations are as follows:

1. Stainless steel- nitric acid
2. Nickel and Nickel alloy- caustic
3. Monel-hydrofluoric acid
4. Hastelloys(Chlorimets)-hot hydrochloric acid
5. Lead-dilute sulfuric acid
6. Aluminum-nonstaining atmospheric exposure

7. Tin-distilled water
8. Titanium-hot strong oxidizing solutions
9. Tantalum-ultimate resistance
10. Steel- concentrated sulfuric acid

2.1.4.2 Anodic Protection:

It is one of the more recently developed electrochemical methods of corrosion control. Anodic protection has been used most extensively in the pulp and paper industry to protect equipment like storage vessels, process reactors, heat exchangers, and transportation vessels for storage and handling of sulfuric acid as well as digesters and storage tanks holding green and white kraft liquors. It can be used to control the corrosion of metals in chemical environments that exhibit very interesting behavior when subjected to anodic polarization. This behavior can be studied with an experimental setup, which is shown in block-diagram fashion in Fig.2.1. When the potential of the working electrode relative to the reference electrode is controlled and shifted in the more anodic (positive) direction, the current required to cause that shift varies. If the current required for the shift has the general behavior with respect to potential shown in the Evans diagram in Fig. 2.2, the metal is termed active-passive and can be anodically protected. Few systems exhibit this type of behavior. Some metals and solutions that have been found to have active-passive properties and can be anodically protected include:

| Metal | Solutions |
|--|---|
| <ul style="list-style-type: none">• Steels | <ul style="list-style-type: none">• Sulfuric acid |
| <ul style="list-style-type: none">• Stainless steels | <ul style="list-style-type: none">• Phosphoric acid |
| <ul style="list-style-type: none">• Nickel | <ul style="list-style-type: none">• Nitric acid |
| <ul style="list-style-type: none">• Nickel alloys | <ul style="list-style-type: none">• Nitrate solutions |
| <ul style="list-style-type: none">• Chromium | <ul style="list-style-type: none">• Aqueous ammonia• Organic acids |

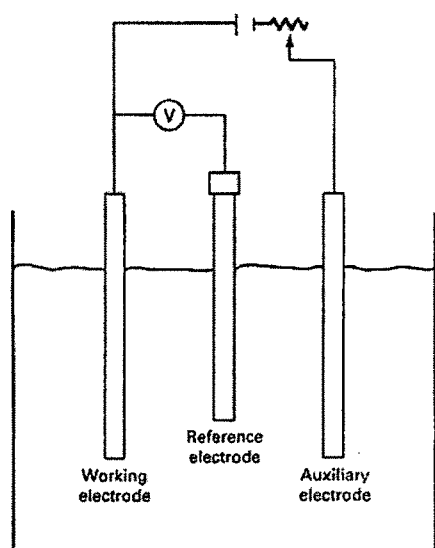


Fig. 2.1 Schematic of experimental apparatus used for anodic polarization studies

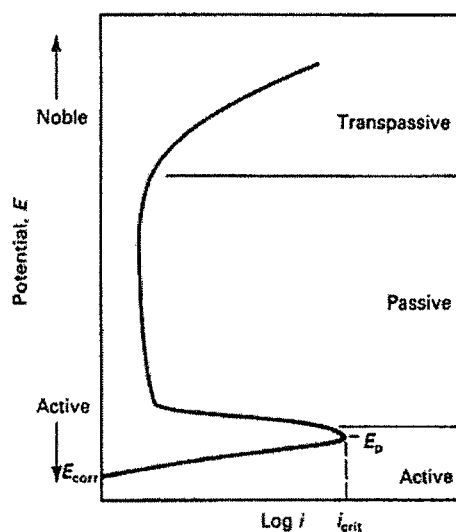


Fig. 2.2 Schematic anodic polarization curve

The corrosion rate of an active-passive metal can be significantly reduced by shifting the potential of the metal so that it is at a value in the passive range shown in Fig. 2.2. The current required to shift the potential in the anodic direction from the corrosion potential, E_{corr} , is several orders of magnitude greater than the potential at a passive value. The current peaks at the primary passivation potential value, shown as E_p (Fig. 2.2). Anodic protection can be used to form the passive film on metals in chemical systems that would normally be corrosive; at other times, anodic protection can be used to maintain the passivity of the metal, so that the process changes do not force the metal to become active and corrode [6].

2.1.4.3 Cathodic Protection

It is an electrochemical means of corrosion control in which the oxidation reaction in a galvanic cell is concentrated at the anode and suppresses corrosion of the cathode in the same cell. Using an externally applied electric current, corrosion is reduced essentially to zero. A metal surface that is cathodically protected can be maintained in a corrosive environment without deterioration for an indefinite time. There are two types of cathodic protection: impressed current cathodic protection (ICCP) and sacrificial anode cathodic protection (SACP), also known as galvanic cathodic protection.[7]

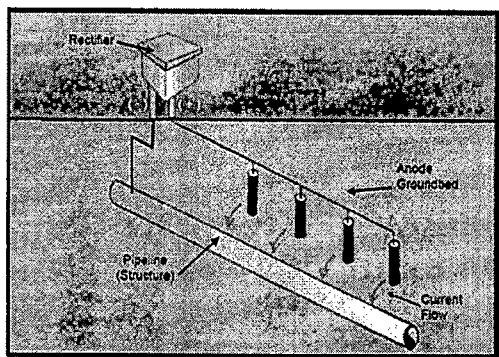


Fig 2.3 protected buried pipeline by Impressed Current System

Cathodic protection requires a source of direct current and an auxiliary electrode (anode) usually of iron or graphite located some distance away from the protected structure. The direct current (dc) source is connected with its positive terminal to the auxiliary electrode and its negative terminal to the structure to be protected; in this way, current flows from the electrode through the electrolyte to the structure. The applied voltage is not critical — it need only be sufficient to supply an adequate current density to all parts of the protected structure. In soils or waters of high resistivity, the applied voltage must be higher than in environments of low resistivity. Or, when the extremities of a long pipeline are to be protected by a single anode, the applied voltage must be raised

2.1.4.4 Modifying Environment-Inhibitor

An inhibitor is a chemical substance that, when added in small concentration to an environment, effectively decreases the corrosion rate. A corrosion inhibitor may act in a number of ways: it may restrict the rate of the anodic process or the cathodic process by simply blocking active sites on the metal surface. Alternatively it may act by increasing the potential of the metal surface so that the metal enters the passivation region where a natural oxide film forms. A further mode of action of some inhibitors is that the inhibiting compound contributes to the formation of a thin layer on the surface which stifles the corrosion process. There are several classes of inhibitors, conveniently designated as follows: (1) passivators, (2) organic inhibitors, including slushing compounds and pickling inhibitors, and (3) vapor - phase inhibitors.

2.1.4.5 Metal coatings

Metal coatings are applied by dipping, electroplating, spraying, cementation, and diffusion. The selection of a coating process for a specific application depends on several

factors, including the corrosion resistance that is required, the anticipated lifetime of the coated material, the number of parts being produced, the production rate that is required, and environmental considerations.

2.1.4.5.1 Hot dipping Galvanizing:

It is carried out by immersing the metal on which the coating is to be applied, usually steel, in a bath of the molten metal that is to constitute the coating, most commonly zinc, but also aluminum and aluminum – zinc alloys. Hot dipping can be either a continuous process, as in galvanizing steel sheet, or a batch process — for example, galvanizing fabricated parts, nuts, bolts, and fasteners.

2.1.4.5.2 Electrogalvanizing

It is the electroplating of zinc on either iron or steel. Electroplated zinc - coated sheet is widely used for exposed automobile body panels because of its uniform coating thickness and surface characteristics compared to hot - dip zinc - coated. Coatings range in thickness from 4 to 14 μm .

2.1.4.5.3 Electroplating :

The substrate, or base, metal is made the cathode in an aqueous electrolyte from which the coating is deposited. Although the primary purpose of electroplating coatings is to achieve corrosion resistance, these coatings can also be decorative, with a metallic luster after polishing. A wide variety of coatings can be applied by electroplating — for example, zinc, cadmium, chromium, copper, gold, nickel, tin, and silver, as well as alloys, such as tin – zinc, zinc – nickel, brass, bronze, gold alloys, and nickel alloys.

2.1.4.5.4 Electroless plating

Coatings are also produced by chemical reduction of metal – salt solutions, with the precipitated metal forming an adherent overlay on the base metal. Nickel coatings of this kind are called *electroless* nickel plate.

2.1.4.5.5 Thermal spraying

Gun is used that simultaneously melts and propels small droplets of metal onto the surface to be coated. There are several types of thermal spraying, with the three main variables in each type being the temperature of the flame, the velocity of the particles that are sprayed onto the substrate to form the coating, and the nature of the material that is to form the coating (i.e., powder, rod, wire, or liquid). The material that is to form the

coating is called the “feedstock.” In all cases, the feedstock is rapidly heated and propelled toward the substrate where, on impact, it consolidates forming an adherent coating. In flame - powder spraying, powder feedstock is melted and carried by the flame onto the work piece. In flame - wire spraying, the flame melts the wire, and a stream of air propels the molten material onto the work piece. In plasma spraying, a plasma at a temperature of about 12,000 ° C is formed, and the plasma stream carries the powder feedstock to the work piece [9].

2.2 Fundamentals of Overlay or Cladding

2.2.1 Definition of Cladding:

Cladding is a process to deposit a fine layer of a material using strip or filler electrode that is fused under an agglomerated flux onto a non-alloyed or low-alloy base material to get good corrosion resistance, wear resistance & high hardness surface. The weld metal properties of the cladding are mainly determined by the chemical composition of the deposit which can be obtained with several different combinations of strip or electrodes, fluxes and welding parameters.

2.2.2 Why cladding is required?

Large pressure vessels are used in hydrogen containing environments, for example, in the petroleum industry in hydrocracking, hydrodesulphurization and catalytic reforming processes as well as in the chemical and coal conversion industries. Many reactor vessels operate at high temperatures and at high hydrogen partial pressures, with 450°C and 15 MPa. The vessels are generally fabricated from low alloy, creep resistant steels which have good strength and structural properties but very low corrosion resistance [10].

- In chemical industries or petrochemical industries, it is difficult to resist the effect of corrosion in a highly corrosive atmosphere of hydrocarbons.
- stainless steel having very good corrosion resistance but it is very costly.
- So, applying stainless steel or Inconel overlay on the inner surface of Carbon/Low alloy steel vessels economically serves both the purpose – required mechanical properties and good corrosion resistance properties[11].

2.2.3 Types of overlays

- Hard-facing overlays
- Corrosion resistance overlays

▪ **Hard facing overlays**

Hard facing is a form of surfacing that is applied for the purpose of reducing wear or abrasion, impact, erosion, galling, or cavitations of piping, valves, fittings or similar components. For strength, corrosion, abrasion or erosion criteria, various alloys must be chosen over low carbon steel.

▪ **Corrosion resistant Overlays**

Corrosion resistance overlay is a layer of weld metal applied to a carbon or low alloy steel base metal for the purpose of providing a corrosion resistant surface when that surface is to be exposed to a corrosive environment. The corrosion resistance of a substrate can be improved by metallurgical bonding to the susceptible core alloy a surface layer of a metal or an alloy with good corrosion resistance. The cladding is selected not only to have good corrosion resistance but also to be anodic to the core alloy by about 80 to 100 mV [12]. Compared to carbon and alloy steels, all corrosion resistant alloys are expensive. Cladding can save up to 80% of the cost of using solid alloy. Clad materials are widely used in the chemical process, offshore oil production, oil refining and electric power generation industries.

2.2.4 Different Routes to obtain a clad material:

- clad plates produced by rolling which are mostly only available in standardised dimensions and grades.
- explosion clad plates.
- clad plates made by weld overlay

2.2.5 Commonly used welding processes for Weld overlays or cladding

Following different welding process can be used for corrosion resistance weld overlays.

1. SMAW (Shielded metal arc welding)
2. SAW (Submerged Arc Welding)
3. FCAW (Flux cored Arc welding)
4. PAW (Plasma Arc Welding)
5. ESSC (Electroslag strip cladding)

2.2.6 Weld Cladding process Applicability

- SMAW-Shielded metal arc welding. Application to small components and repairs of clad.
- SASC-Submerge arc strip cladding. Applicable to flange to large inside area of shell, dished ends, and tube sheet.
- FCAW-Flux cored arc welding. Applicability to large flange face, Small size tubesheet, pipes of smaller diameter.
- MIG-Metal inert gas welding .Applicable to flange face, small size tube sheet, pipes of smaller diameter.
- ESSC- Electro slag strip cladding. Applicable to large inside area of shell, Dished ends, Cone, and Tube sheet.[13]

2.2.7 Introduction of strip cladding Processes:

Stainless steel strip cladding is a flexible & economical way of depositing corrosion resistant, protective layer on low alloy or low carbon steel due to which it is widely used in the production of components for chemical, petrochemical & nuclear industries [14]. Large pressure vessels are used in hydrogen containing environments, for example, in the petroleum industry in hydro-cracking, hydrodesulphurization and catalytic reforming processes as well as in the chemical and coal conversion industries [15]. Many reactor vessels operate at high temperatures and at high hydrogen partial pressures, with 450°C and 15 MPa often being mentioned as typical values. The vessels are generally fabricated from low alloy, creep resistant steels [16-17]. All hydro processing reactors require internal protection of the reactor vessel walls to resist the high temperature corrosion due to presence of sulphur in the process stream. This protection is generally provided by stainless steel strip electrodes which are made up of different grade such as 347, 309L, 309LNb, 316L, 317L. A stabilized composition overlay also prevents sensitization during the final post weld heat treatment (PWHT) cycle of the reactor. The two most productive systems for surfacing large components which are subjected to corrosion or wear are submerged arc and electroslag cladding, using a strip electrode. Both processes are characterized by a high deposition rate, low dilution and high deposit quality, and they are both suitable for surfacing flat and curved objects such as heat exchanger tube sheets and pressure vessels. Submerged arc welding (SAW) is most frequently used but, if higher productivity and

restricted dilution rates are required, electroslag welding (ESW) is recommended. The principle of strip cladding was developed in the USA around 1920 but in Europe the process retained detailed attention when the nuclear industry started (late 1950's). The nuclear power industry needed a method whereby thick- wall pressure vessels could be given a corrosion resistant inner surface.[18].The electroslag process was invented by H K Hopkins of the M W Kellogg Company in 1936. At that time stainless clad plate was being produced by making submerge arc weld deposit of the required composition on one side of slab and then rolling out into plate. The system work well for 12Cr cladding but with 18Cr 8Ni types the weld deposit cracked. Hopkins therefore stood the slab on end and applied the weld metal by traversing to and fro and at the same time moving upwards. In 1971, Seidel and Hass reported a new adaptation of electroslag processing for cladding in the flat position using strip electrodes and called it electroslag surfacing. Ten year later, this concept was also utilized by Nakano in Japan to develop Kawasaki's electroslag surfacing techniques called "Maglay" in which 150 mm wide strip was used. This process employ Joules heating of slag instead of arc as welding heat source which results in decreasing dilution ratio about 10 %.[19]

2.3 Description of The ESSC Process

2.3.1 Basic Principle of the ESSC

Electroslag strip cladding is a development of submerged arc strip cladding which has established itself as a reliable high deposition rate process. The principle of this process has been known for a number of years and publications concerning its fundamentals were first published in the early seventy's. The process is initiated by starting an electric arc between the electrode and the base metal which results in initial melting the flux. The Molten slag became electro conductive due to the presence of special ingredient and it will support the passage of current at lower voltage and the arc gets extinguished. [20] . As soon as sufficiently thick layer of molten slag is formed, all arc action stops .A strip electrode is continuously fed into a shallow layer of molten electro conductive slag. The heat which is needed to melt the strip, slag forming flux and the surface layer of base metal is generated by the Joule effect as a result of the welding current flowing through the liquid electro conductive slag.

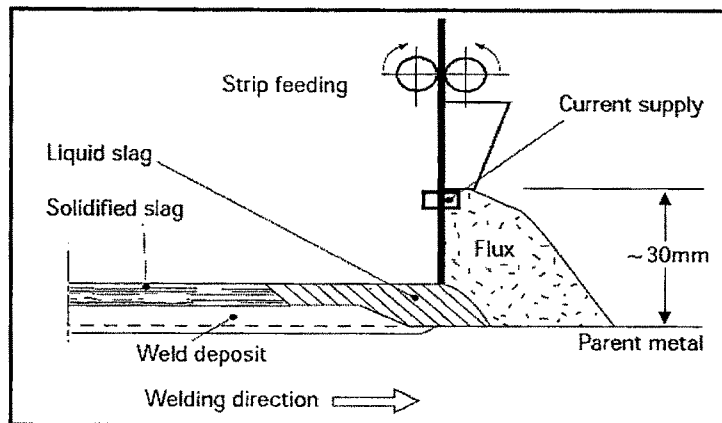


Fig.2.4 Schematic Diagram of ESSC Process

Heat generated by the resistance of the molten slag to passage of the welding current is sufficient to fused the surface of the work piece and the strip electrode. The interior temperature of the bath is in vicinity of 1925°C while the surface temperature is approximately 1650°C . Melted electrode and the base metal collect in pool beneath the molten slag bath and slowly solidify to form the clad.

The resistance at the arc is determined by the properties of the filler and the base materials as well as by the temperature and ionization parameters. The resistance in the slag results from the resistance in the slag materials together with the interface resistances at the boundaries between the filler and the slag and the slag and the base material. Due to much greater area of the combined contact surfaces between the slag and the base materials ,the interface resistance here is so small as to negligible, so that the flowing applies

$$R_{\text{slag}} = R_x + R_{\text{melt}}$$

$$R_{\text{slag}} = \text{Resistance in the slag}$$

$$R_x = \text{Resistance at interface}$$

$$R_{\text{melt}} = \text{Resistance in the molten metal pool}$$

In the SAW process the slag-current is lost due to the nature of the process which can be reduce in ESSC by reducing the thickness of the slag layer and size of the electrodes but this lost cannot completely eliminated[21].

In ESSC process, the arc must be extinguished once it has been ignited and the current flow through the slag. As a consequence, the following must apply:

$$RA \geq \infty, IA = 0$$

Where , RA = Resistance in the arc and IA = Current in the arc

If these conditions are to be satisfactory, the electrical resistance for the slag must be less than that for the arc. This presupposes that the electrical conductivity of the liquid slag created during the ignition, process will rise with the rising temperature or, the specific resistance is dependent on the temperature and is going down with rising temperature. If the process is to be stable, the thickness of the layer and the surface of the slag pool must be kept constant. This is affected by continuously melting flux, which is fed at one side only. To retard the interface resistance; it is important that the strip electrode has a sufficient depth in the slag pool. In ESSC process the resistance heating of the slag melts the fillet metal and the base material. Electroslag surfacing is thus classified as a resistance welding technique.

2.3.2 Characteristics of ESSC

- Electro-slag strip cladding is the modified version of submerged arc strip cladding process.
- The heat generation in the case of ESSC is due to the current flowing through the electro-conductive slag.
- Molten weld pool will be visible during welding.
- Radiation only in the visible and infrared spectrum. No ultraviolet radiation because of the absence of the arc.
- Flux fed from front side only.
- Automatic removal of the slag crust.
- Very regular, finely ripped bead, without any slag adherence.
- Because of low penetration and newly developed strip / flux combination low carbon stainless steel deposits can be achieved in single layer .
- Low arc voltage (24 – 26V)
- Can be applied on curved as well as flat surfaces.
- Low heat input in parent metal.
- Low flux consumption. (0.4 -0.5 Kg/Kg strip).
- Increased welding speed (50% - 200 % higher), resulting in higher area coverage in m²/h.
- Suitable for depositing both corrosion resistant and wear resistant weld metal.

2.3.3 Comparison of ESSC with SASC process

Table-2.1: Comparison of ESSC with SASC process of basic features

| Electroslag Strip Cladding | Submerged Arc Strip Cladding |
|--|--|
| Energy required to melt the strip, the base metal and the flux is produced by Joule effect. i.e it is arcless process. | Energy required to melt the strip and the base metal is supplied by the electric arc struck between them. |
| The agglomerated flux is fed from the one side only to protect the liquid metal and where applicable enriches it with alloying elements. | The agglomerated flux is fed from both the side to protect the liquid metal and where applicable enriches it with alloying elements. |
| High rate of deposition than SASC | Low rate of deposition than SASC |
| Dilution is reduced by 50 % with respect to SARC | Dilution is low but with respect to ESSC is high. |
| Low penetration level | Low penetration level |
| Strip is used having widths in the ranges of 30 to 120 mm. | Strip is used having widths in the ranges of 30 to 90 mm. |
| Flux consumption is low with respect to SASC | Flux consumption is high with respect to ESSC. |

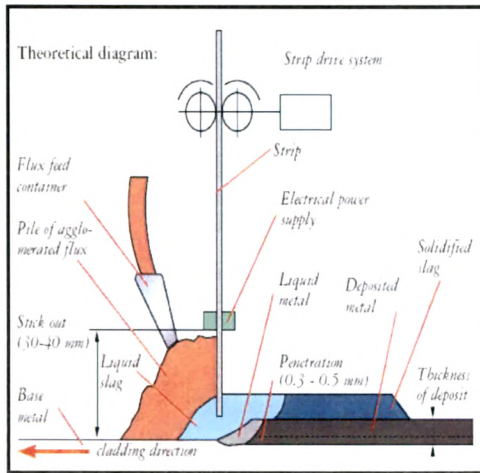


Fig.2.5 Line Diagram of ESSC Process

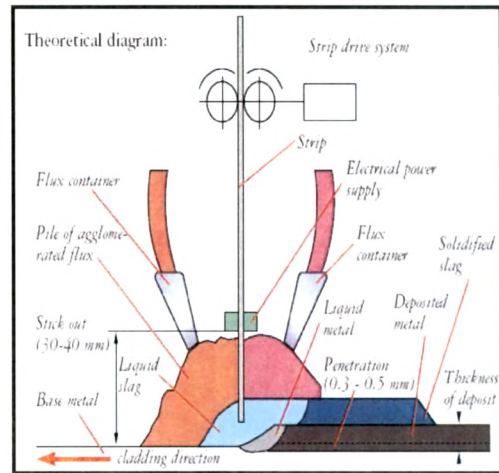


Fig.2.6 Line Diagram of SASC Process

Table-2.2: Comparison of welding parameters of ESSC with SASC

| Welding Parameters | SASC Process | ESSC Process |
|-------------------------------------|--------------|--------------|
| Strip Dimensions(mm) | 60 x 0.5 | 60 x 0.5 |
| Current(A) | 750 | 1250 |
| Voltage(V) | 26 | 24 |
| Travel Speed(cm/min.) | 10 | 16 |
| Magnetic Control | No | Yes |
| Cladding Energy(kj/cm) | 117 | 112.5 |
| Cladding Thickness | 4.5 | 4.5 |
| Dilution(%) | 18 | 9 |
| Deposition Rate(Kg/h) | 14 | 22 |
| Flux Consumption(Kg flux/ Kg strip) | 0.7 | 0.5 |

2.3.4 Advantages of the Electroslag strip cladding process :

- Low dilution by the base metal
- Higher melting rate (R_{melt})
- Higher deposition rate (R_{dep})
- Low flux consumption
- Smooth bead surface with a higher degree of purity .[22]

2.3.5 Limitations of the Electroslag strip cladding process :

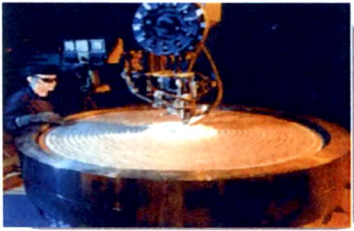
- Weld in the flat or downhand position
- Adequate access for the welding head
- The overlap between adjacent beads must be controlled to avoid lack of fusion defects.
- The chemical composition & welding parameters of the strip must be carefully selected to take into account the level of dilution[23].

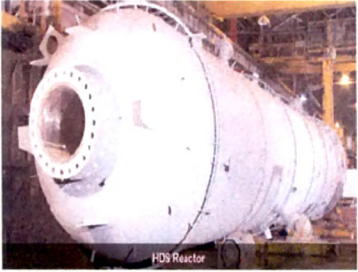
2.3.6 Application of Electroslag Strip Cladding Process

- Nuclear Power Components (marine environments)
- Petro Chemical Industry (High temp, high pressure)
- Chemical industry. (High temp, high pressure)

- Offshore Industry. (seawater environments)
- Paper industry. (aggressive service environments.)
- See Water Desalination Plants. (seawater environments)
- Waste Water processing
- Desulphuration Plants. (acidic environments)
- Surfacing of Continuous Casting Rollers. (high pressure)

Table 2.3 : Industrial application of ESSC Process[24,25]

| Oil, Gas & Petrochemical Industries | | | | |
|-------------------------------------|---|---|--|---------------------------------------|
| Sr. No | Component to be clad | service condition | Base metal | Clad Metal |
| 1 | Tubes and pipes for heat exchangers  | -seawater or chlorinated seawater as coolant - contaminated with hydrochloric acid | Cr-Mo Steel | Duplex stainless steel Sandvik SAF 25 |
| 2 | Hemispherical end section of Pressure vessel  | Hydro cracking operating temperature 450 ⁰ C, 15 MPa H ₂ partial pressure | 2 ¼ Cr-1Mo alloy, V modified 2 ¼ Cr-1Mo , 3 Cr- 1 Mo Steel | 309 L & 347 |
| 3 | Hydro cracker reactor  | Hydro cracking operating temperature 450 ⁰ C, 15 MPa H ₂ partial pressure | SA336 F12 | 347 |

| | | | | |
|----------|--|--|---|-----------------|
| <p>4</p> | <p>Hydro-desulphurization reactor</p>  | <p>270⁰ C & 40 Bar Pressure, 650 – 750⁰ C</p> | <p>2.25Cr-1Mo pressure vessel steel</p> | <p>347</p> |
| <p>5</p> | <p>Bolw Valve</p>  | <p>deep-water, pre-salt and sour-service environments</p> | <p>Low alloy steel</p> | <p>347 ,321</p> |
| <p>6</p> | <p>Dish end of condenser or separator</p>  | <p>Water with some salts</p> | <p>Mild steel P355NL1</p> | <p>316 L</p> |
| <p>7</p> | <p>Hydrodesulfurization(DHDS)/ Reactor</p>  | <p>operating tempaure 389- 414⁰ C & 89 Bar removal of suphur dioxide with by reaction with ammonium sulfate & also produce a ammonium sulfite crystal(fertilizer byproduct)</p> | <p>SA 387 Gr 11 c 12 (Cr-Mo-V)</p> | <p>347</p> |

| Shipbuilding | | | | |
|------------------------------------|---|--|-------------------|--|
| Sr. No | Component to be clad | service condition | Base metal | Clad Metal |
| 1 | Main propeller shafting,  | chloride-containing | Low alloy steel | 308 L, Inconel 625, |
| Pulp & Paper industries | | | | |
| Sr. No | Component to be clad | service condition | Base metal | Clad Metal |
| 1 | Fibre flow drum  | chloride-containing bleaching environments | Mild steel | 309 L |
| Nuclear power plants | | | | |
| Sr. No | Component to be clad | service condition | Base metal | Clad Metal |
| 1 | Reactor pressure vessels  | Water as coolant | low-alloy steel | ,308 L,308 L Nb ASS (19.% Cr,10.7% Ni) |

2.3.7 Welding Equipment

2.3.7.1 Power sources

In view of keeping the strip feed rate and voltage variations within very narrow limits imposed with regard to the shallow depth of the slag pool, it is advised to use DCCP rectifiers. Since the electroslag process requires average optimised current densities of approx 40 A/mm^2 , the output of the power sources at a 100% duty cycle has to meet high

amps such as 1250 A for a 60 mm strip (typical). In practice to obtain the required current intensity levels two power sources can be connected in parallel. It should be checked with the manufacturer whether given DCCP power sources can be connected in parallel without any additional precautions. To obtain optimum welding conditions and bead profile, it is necessary to use a power source which will give stable voltage outputs between 21 – 27 volts.[23]

2.3.7.2 Welding Heads

The function of the welding head is to feed the strip at a constant speed which is related to the welding parameters. The strip feed rates for the electroslag process range from 1 to 2,5 m/min. In practice no special welding heads are required to carry out electroslag strip cladding.[23]

2.3.7.3 Strip Feeding Nozzles

The main functions of the feeding nozzle are to guide the strip and to maintain it in the required position during the welding operation and to transfer the welding current from the power source to the strip by means of appropriate contact shoes. There is no fundamental difference in design between the sub arc and the electroslag feeding nozzle, however because of the high current densities involved, and due to the fact the rear side of the electroslag is subject to the heat radiation from the slag pool, their construction is generally somewhat heavier. The electroslag nozzle is also equipped with a water cooling possibility. [23]

2.3.8 Magnetic Steering Device

As mentioned previously, the slag pool is electroconductive, therefore, the slag pool is subjected to electromagnetic forces which tend to make it flow from the sides towards the centre of the molten pool. This results in narrower beads, more unfavorable wetting angles resulting in a more difficult slag removal and increased risks from undercut.

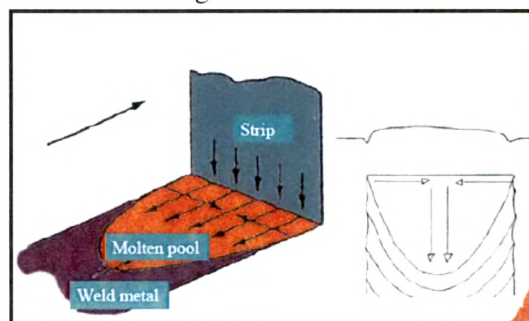


Fig.2.7 Undercut caused by welding current

The fluid force F (dyn/cm) created by welding current is as follows:

$$F = iB = i\mu_0 H$$

I = Line density of current (amp/cm)

B = Magnetic induction (G)

μ_0 = Magnetic permeability (H/m)

H = Magnetic field intensity (A/m)

In this case H is a function of positive r from an electrode end to the inside and obtained by equation

$$H(r) = \frac{1}{2\pi} \left(\frac{I}{W} \right) \int_r^{W-r} \frac{dr}{r}$$

where, I = Welding current (A)

W = Electrode width (cm)

$$= \frac{1}{2\pi} \frac{I}{W} \ln \left(\frac{W-r}{r} \right)$$

To compensate this phenomenon, are used in which an external magnetic field generating forces of the same nature is applied but in the opposing direction and equal to slightly in excess of this fluid force. The external magnetic field is created by means of two solenoids. Fig. 2.8 shows magnetic steering devices with solenoids which is fitted onto the cladding nozzle, the current cables and the steering control box [26].



Fig. 2.8 Magnetic steering devices with solenoids.

The location of the solenoids are very important. The tips should be placed beside the strip electrode at a distance of approx 15 mm from the strip edge and about 15 mm above the base material surface.

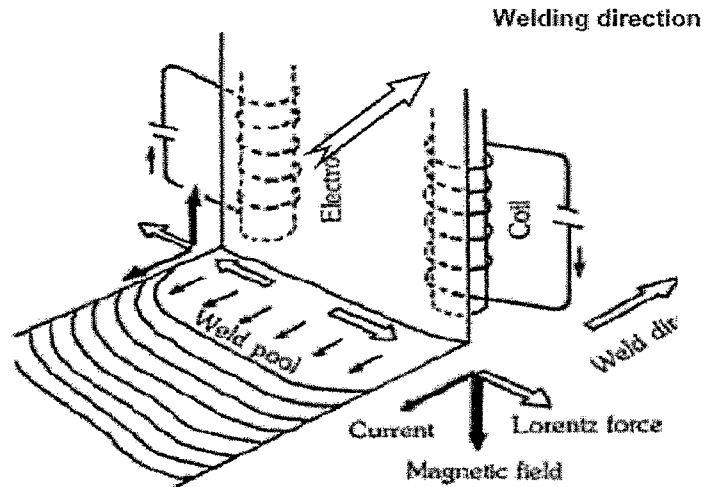


Fig.2.9 Control of slag flow with outer magnetic field

The external magnetic field is utilized to control flow direction and velocity of the fused slag and fused metal. This principle is shown in fig. 2.9 Lorentz force is generated by the interaction between the external magnetic field perpendicular to the parent metal and welding current, and the force from the center of the molten pool to its edges supplies the fused slag and fused metal to the edges.

2.3.9 Welding Parameters

2.3.9.1 Current:

Due to absence of an arc, the penetration in the ESSC process is very shallow; this means that there will be little mixture of the filler metal with the melted base material. It is possible in comparison with submerged arc welding, to use far higher power levels. The current level is the single most important factor controlling the deposition rate in the electrosag process. Both deposition rate and penetration rate are found to increase with current in a linear manner –fig. 2.10.

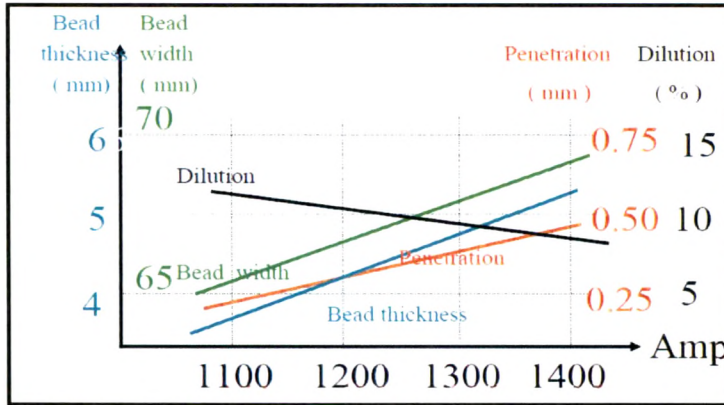


Fig .2.10 Effect of current on Dilution, Bead with, Penetration, Bead thickness

Welding parameters: voltage = 24 V, Travel speed = 15 cm/mm, Stick out = 30 mm

Since the dilution is dependent upon the deposition rate and penetration, the combine effect s of both factors resulted in variation in the dilution. The slight drop in dilution with increasing current can be explained by the interaction between growth in bead thickness, width and penetration. At the low current density , the surfacing layer developed undercutting, while excessive current density had either the short circuit at low voltage or the melt back at high voltage[27].

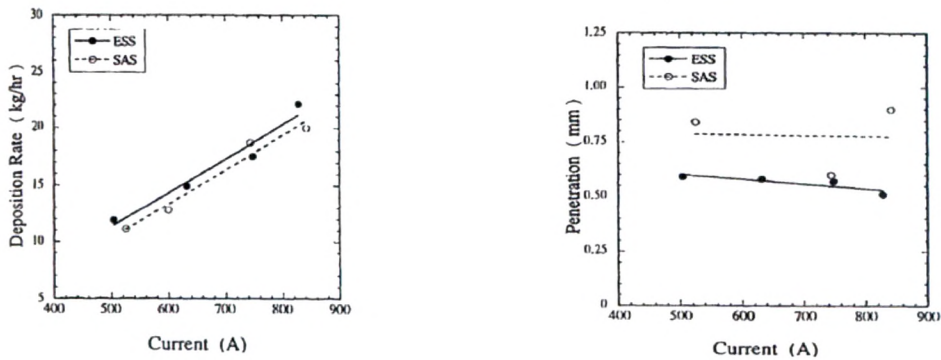


Fig.2.11 The effect of current on the deposition rate and penetration of cladding deposited on MIL-S- 23284 class 1 steel using 30 by 0.5 mm strip of Ni alloy 625.

Due to low penetrating effect of the electroslag welding process, for thick layers it is possible to use current density 42 A/ mm^2 without any appreciable dilution (e.g 1250 A for $60 \times 0.5 \text{ mm}^2$ strip) and for relatively thin layers ($< 4\text{mm}$), It is preferable to keep the current density 33 A/ mm^2 (e.g 1000 A for $60 \times 0.5 \text{ mm}^2$ strip).To work on such thin layers with high current requires such a high travel speed that the strip electrode fully or

partly rides forward out of molten slag, resulting in sharp increase in arcing ,hasty welding on the both sides of the head. This problem is more pronounced with wider strips because of large current used. By employing a magnetic control device the undercut problem can be eliminated. When using wider strip electrodes -120 x 0.5 mm current of greater than 2500 A may be required [28].

2.3.9.2 Welding Voltage:

The welding voltage should be accurately control because it affects the specific resistance of the liquid slag and will determine how far the strip electrode is to be submerged in the slag pool. Insufficient immersion in the weld pool will cause the process to become unstable. The welding voltage must be lowered as current rises. A range of 24 to 26 V when operating at 1250 A, or 22 to 24 V for 2500 A, is normal. At voltage below 24 V, the strip electrode has tendency to strike to the base metal and resulting in short circuiting and hence the process become unsuitable. At above 26 V, the amount of slag spatter increases rapidly while at about 28 V and above it the process started arcing on the surface of the flux and slag spatter become violent. The exact value will depend on the properties of the flux and the dimensions of the strip. At given welding current and welding speed, the dead thickness and width and penetration / dilution of the base metal vary with the voltage shown in the fig. 2.11.

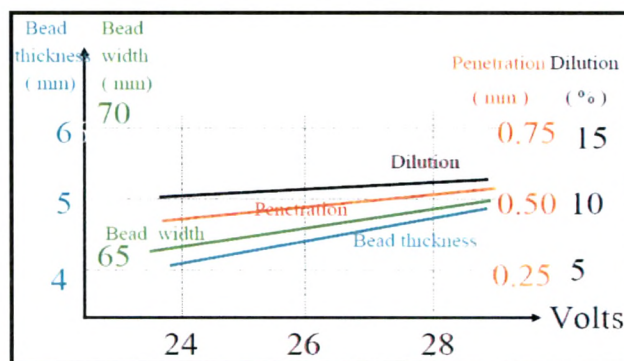


Fig .2.12 Effect of welding voltage on Dilution, Bead width, Penetration and Bead thickness.

The slag spatter tendency can also be controlled by depth of flux, but in order to maintain the flux consumption at lowest possible level, the depth of the flux burden should not exceed 35 mm.

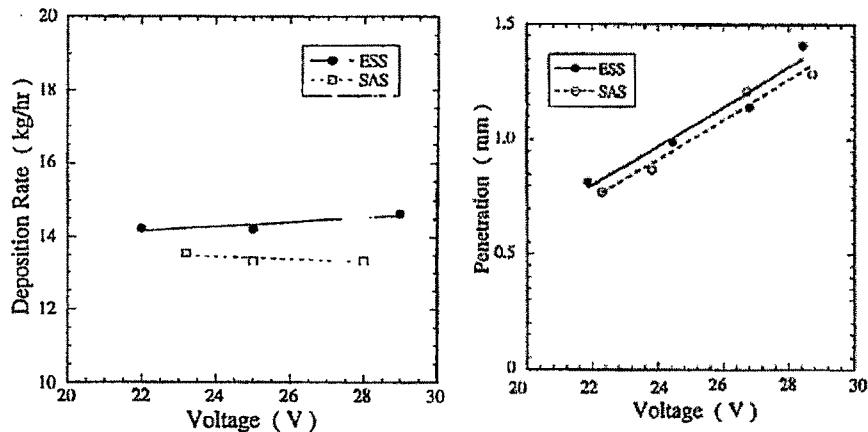


Fig.2.13 The effect of voltage on the deposition rate and penetration of cladding deposited on MIL-S- 23284 class 1 steel using 30 by 0.5 mm strip of Ni alloy 625.

Arcing may be experienced if the voltage is too high and the electrode is not immersed far enough in the slag pool. The welding process becomes unstable with increased arcing.

2.3.9.3 Welding Speed:

The electroslog strip cladding process was stable only when sufficient contact area between the molten slag pool and the melting strip was maintained. An excessive fast travels speed caused the strip to be in contact with insufficiently heated slag, thus resulting in sporadic submerged arcing and process instability. Excessive travel speed resulted in not only an overlay thickness but also the formation of undercutting. On the other hand, too slow a travel speed resulted in bead thickness increase with an accompanying wetting angle so steep that slag entrapment may occur at the bead overlaps[29]. At given welding current and voltage, the bead thickness, bead width and penetration or dilution of the base metal vary with welding speed as illustrated by fig.2.14. The welding speed has a considerable influence on bead geometry and dilution. The increasing welding speed can be explained by the interaction between decreased bead thickness, width and increased penetration. Heat transferred to the base metal is influenced by the relative location of the strip electrode and the molten metal pool.

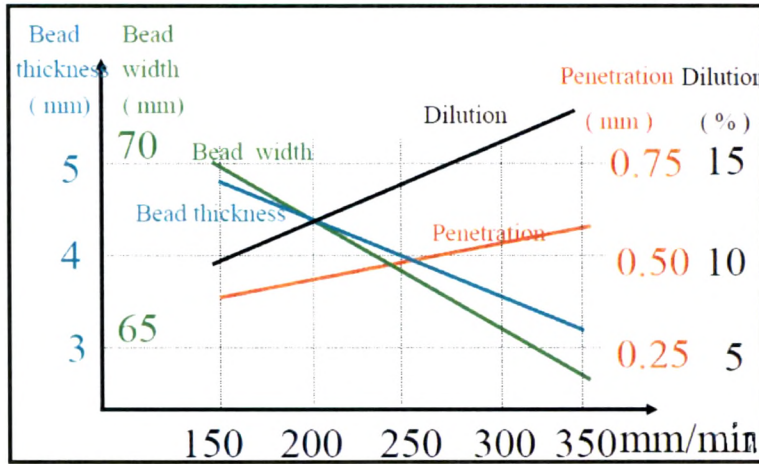


Fig. 2.14 Effect of welding Speed on Dilution, Bead width, Penetration and Bead thickness.

If the electrode is impinged on solid base metal (through the slag), penetration increases, alternatively, if the strip electrode is impinged on previously melted metal, penetration decreases. The deposited metal thickness decreases with increasing travel speed, therefore penetration increases with increasing travel speed, just as it will if electroslag cladding is performed uphill. The dilution greatly increases with increasing travel speed.[30].

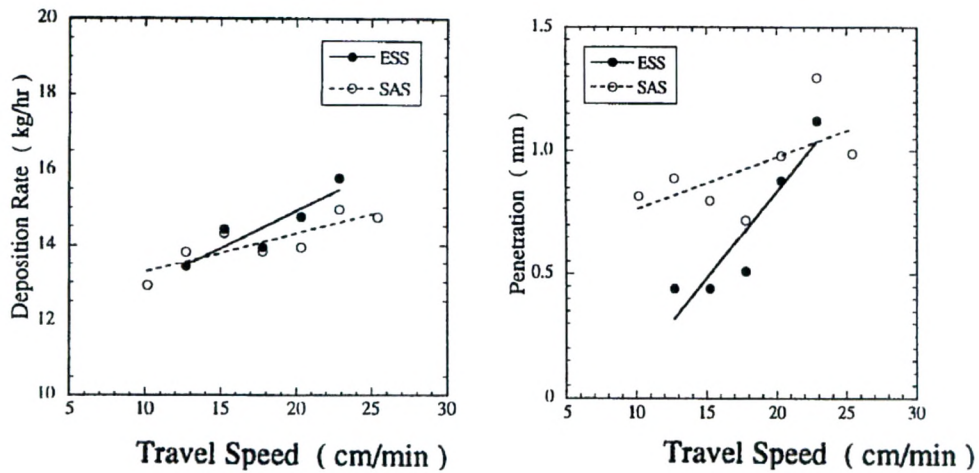


Fig.2.15 The effect of travel speed on the deposition rate and penetration of cladding deposited on MIL-S- 23284 class 1 steel using 30 by 0.5 mm strip of Ni alloy 625.

The travel speed will depend on the desired thickness of the surfacing layer. The greater current density which can be applied along with the high melting rate that can be achieved, make it possible to attain higher welding speeds than would be possible by SAW surfacing. A layer of 4 mm is often specified encountered in processing equipment; the welding speed will be between 160 to 200 mm / min. The extent to which the thickness of the cladding can be reduced by increasing the welding speed is limited since, a speed exceeding 200 mm / min, the strip electrode will tend to run away from the slag pool. For this reason, lower current densities are used to apply thin layers 3.5 mm. Not only can adjusting the welding speed can regulate the surfacing depth; the degree of dilution by the substrate material can also be influenced. In general the optimum travel speed range was about 152 to 203 mm/ min which resulted in about a 11 % dilution level[31].

2.3.9.4 Stick out:

The stick out is the length of the free strips electrode end from the contact jaws to the parent metal. It may vary between 25 and 40 mm without affecting the stability of the process. A variation within this range does not influence bead geometry, penetration or dilution and deposition rate to any large degree. Fig. 2. 16 shows that as stick out is increase the dilution is decreases.

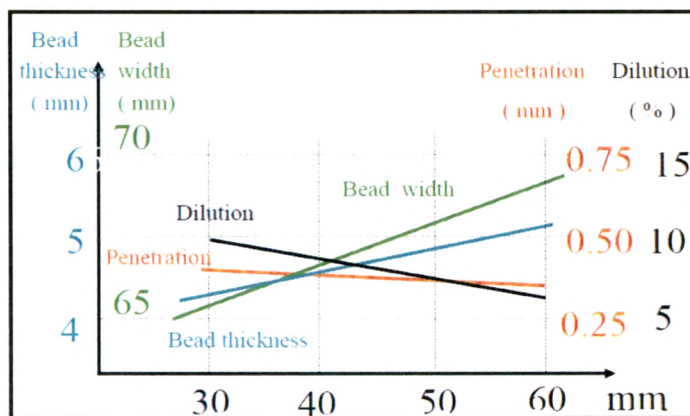


Fig .2.16 Effect of stick out on Dilution, Bead width, Penetration and Bead thickness

2.3.9.5 Dilution:

In weld overlay cladding, our primary concern is to obtain the specified chemistry at a minimum height from the fusion line. However there is a limitation for the this minimum height as some mixing of filler metal with the base metal takes place in weld overlay and it cannot be avoided. This is called dilution. This is controlling factor, which determines the height of weld overlay required for meeting the specified cladding chemistry requirement of the customer.

A low dilution is beneficial because it allows for the desired properties such as wear and corrosion resistance of the surfacing materials to be maintained in the cladding .Dilution is measured by metallographic sectioning transverse to the direction of cladding using the relationship as shown in fig. 2.17.[32] .

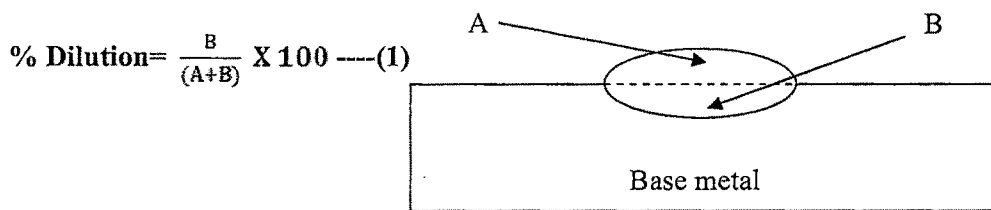


Fig .2.17 Dilution calculation

Where ,

A = cross sectional area of the reinforcement of deposited metal above original surface of the base metal

B = cross sectional area of the melted base metal below original surface of the base metal

It is propose that dilution can be derived from the deposition tare and penetration for electroslog cladding with strip electrodes .from the above dilution equation , the area A, related to the deposition rate can be expressed as:

$$A = R / dV \text{ ----- (2)}$$

where,

d = strip electrode density & V = travel welding speed during ESSC process

Area B can express as :

$$B = PW \text{ -----(3)}$$

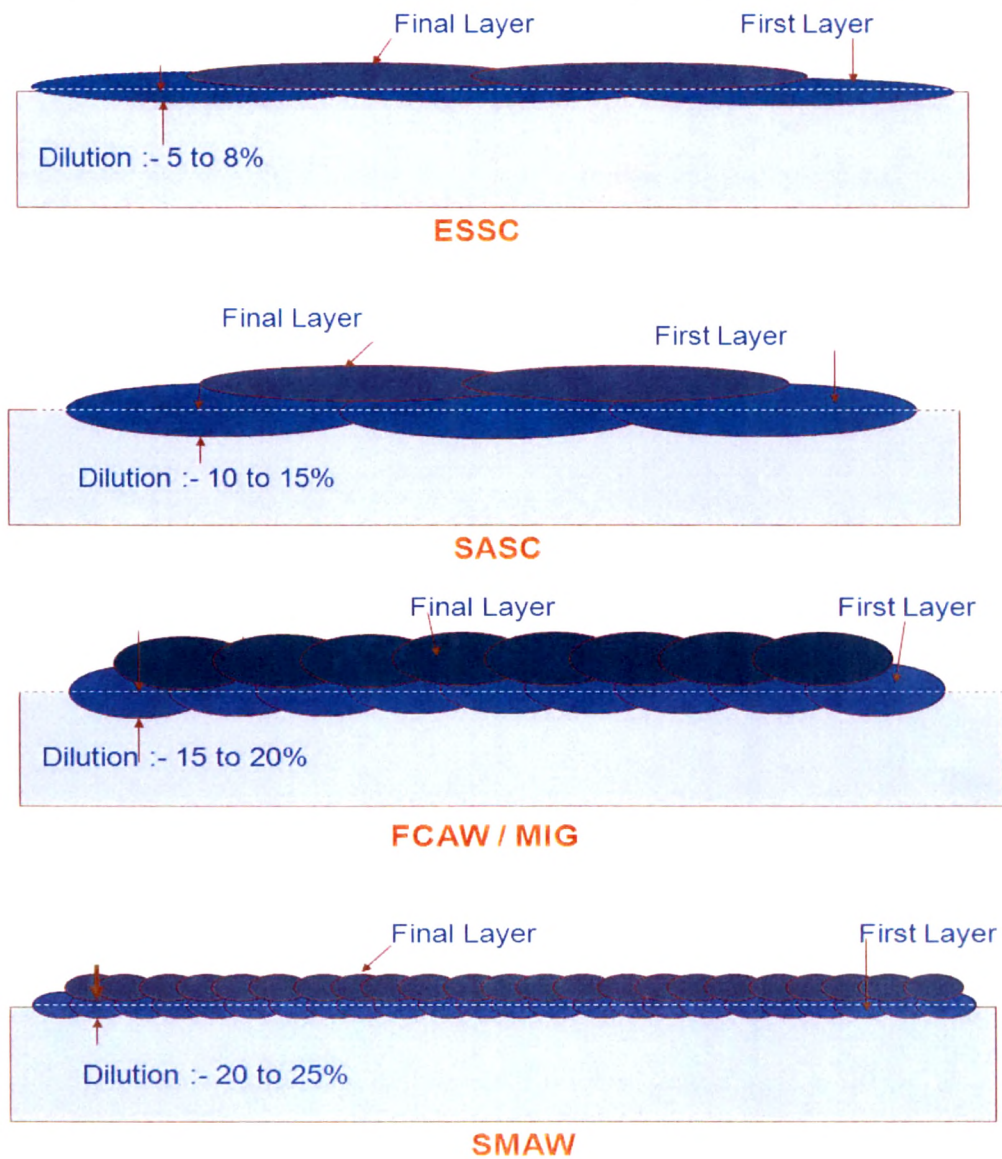


Figure 2.19 Comparative dilution for different processes.

Figure 2.19 shows the comparative dilution for different process, it shows that the ESSC having at least dilution compare to other process[33]

2.3.10 Welding Additives:

2.3.10.1 Strip Electrode:

The standard dimensions for strip electrodes 30 x 0.5 mm, 60 x 0.5 mm and 90 x 0.5 mm, to achieve a given composition in cladding, it will always be necessary to consider the combination of the strip and flux together with the base material. All strip qualities are

cold rolled and have sufficient columnar strength. This is prerequisite for trouble free welding.

2.3.10.1.2 Strip Electrode Composition

ESSC process are mainly use stainless steel and Nickel alloys as strip electrode [35] .

Table-2.4: Stainless steels & Nickel alloys strip for SASC and ESSC process

| Grade | Composition in percentage | | | | | | | |
|------------|---------------------------|-----|-----|------|-------|------|------|-------------------------|
| | C | Si | Mn | Cr | Ni | Mo | N | Other |
| 308L | 0.015 | 0.3 | 1.8 | 20.0 | 10.5 | | 0.06 | |
| 347 | 0.02 | 0.4 | 1.8 | 19.5 | 10.0 | | 0.06 | Nb=0.5 |
| 316L | 0.02 | 0.4 | 1.8 | 18.5 | 13.0 | 2.9 | 0.06 | |
| 2209 | 0.015 | 0.4 | 1.5 | 23.0 | 9.0 | 3.2 | 0.15 | |
| 309L | 0.015 | 0.4 | 1.8 | 23.5 | 13.5 | | 0.06 | |
| 309LNb | 0.02 | 0.3 | 2.1 | 24.0 | 12.5 | | 0.06 | Nb=0.8 |
| 317L | 0.02 | 0.5 | 1.5 | 19.0 | 14.0 | 3.8 | 0.05 | |
| 310MoL | 0.02 | 0.2 | 4.5 | 25.0 | 22.0 | 2.1 | 0.13 | |
| 385 | 0.02 | 0.4 | 1.8 | 20.0 | 25.0 | 4.5 | 0.05 | Cu=1.5 |
| 309L ESW | 0.015 | 0.2 | 1.8 | 21.0 | 11.5 | | 0.06 | |
| 309LNb ESW | 0.015 | 0.2 | 1.8 | 21.0 | 11.0 | | 0.06 | Nb=0.6 |
| 309LMo ESW | 0.015 | 0.2 | 1.8 | 20.5 | 13.5 | 2.9 | 0.06 | |
| 430 | 0.04 | 0.4 | 0.7 | 17.0 | | | 0.06 | |
| NiCr3 | <0.1 | 0.2 | 3.0 | 20.0 | ≥67.0 | | 0.05 | Nb=2.5, Fe≤3.0 |
| NiCrMo3 | <0.1 | 0.1 | 0.3 | 22.0 | ≥58.0 | 9.0 | 0.05 | Nb=4.0, Fe≤2.0 |
| NiCrMo13 | <0.01 | 0.1 | 0.5 | 23.0 | ≥56.0 | 15.5 | | Fe≤1.5 |
| NiCu7 | <0.1 | 1.0 | 3.0 | | 67.0 | | | Cu=29, Ti=2.5 Fe≤2.0 |

2.3.10.1.3 Strip Electrode Thickness:

Strip electrode thickness has great effect on deposition rate, penetration and dilution.

Thin strip electrode can provide slightly increased deposition rate at low current values. But greater productivity is possible with thicker strip at higher current settling because only the thick strip can resist overheating. The penetration slightly decreases with decreasing electrode thickness. One of the reasons is the thin strip electrode produced a greater amount of deposited metal (deposition rate) than did the thick strip electrode for the same heat input.

2.3.10.1.4 Strip Electrode Width

This process favors the use of wide strip electrode to enhance productivity. However wide strip electrodes over 60 mm may develop undercutting. To prevent this, the external magnetic field has been developed to control flow direction and velocity of the fused slag and fused metal.[34].

2.3.10.2 Flux

The welding flux has an influence on a large number of technological and metallurgical characteristics of the deposited metal.

The flux influence various factors such as:

- Operational stability
- the bead profile and wetability
- The slag removal
- the bead appearance
- defect free overlapping
- Regularity of the penetration
- Absence of gas slag inclusions
- Analysis of deposited metal
- Dilution level

2.3.10.2.1 Characteristics of flux powder

- The presence of the earth alkalis increases the arcing characteristics. Even tiny amount of bonding agents in the agglomerated powder e.g Na and K-oxide should be controlled in flux powder.
- May not contain any component, which would create gases like calcium carbonate (CaCO_3) since the gases would interfere with the contact required between the strip electrode and the liquid slag; arcing might result.
- Good electrical conductivity can be achieved by high fluoride content in the powder.
- Its slag should be fluid at a greater distance, behind the electrode and should be detachable and shall not leave any residue on the bead side.
- Should be less hygroscopic so it can bear higher proportion of moisture.

- Must have a melting range lower than the weld metal melting temperature.
- No component of the flux should be volatile at the welding temperature. Preferential loss of any one-flux component during welding leads to variations in weld metal composition along the weld length [36].

2.3.10.2.2 Flux chemistry

Flux used for ESSC, unlike SASC flux, is agglomerated flux in which raw materials are powdered, dry mixed and bonded with ceramic binders. one important property of an electrosag flux is to form a slag steadily conducting electricity through shallow molten pool. This can be achieved by adding large quantities of fluorides, mainly as CaF_2 and NaF and semiconductors as TiO_2 and FeO . The higher the calcium fluorides contains the higher the electroconductivity. Fluorides are preferred as TiO_2 in large quantities improve the slag removal. There was less heat generated with increasing fluoride content. The viscosity of slag was shown to decrease with increasing CaF_2 content. [37].

2.3.10.2.3 Flux particle size and density

The particle size of the flux is controlled to 18 / 60 mesh according to ASTM .i.e min 90 % passes 18 mesh and max 100 % passes 60 mesh. The Flux for ESSC has smaller particle size than atypical flux for SAW- surfacing which generally is calibrated to 14 / 40 mesh. The density of flux is about 0.85 kg/ dm³. It is somewhat lighter than a typical SAW flux which has a density in the range of 0.9-1 kg/ dm³ [38].

2.3.10.2.4 Alloying Vectors:

During the metal transfer through the molten slag pool from the strip electrode end to the weld deposit, changes in chemistry take place owing to metal-slag reactions. Changes in each individual element are expressed as an alloying vector, X_F

$$\% X_F = \% X_{AW} - \% X_S \text{ (5)}$$

X_{AW} = all -weld metal chemistry

X_S = Strip electrode chemistry

If the alloying vectors, dilution of parent metal, strip electrode and parent metal chemistry are known, the weld metal chemistry, X_W , can be calculated by use of the formula:

$$\% X_W = (1-D)(\% X_S + \% X_F) + D X_B$$

X_B = parent metal chemistry

D = dilution of parent metal

The alloying vectors, in percent, for the flux and for a strip electrode with a chromium content of about 20 percent are:

| C | Si | Mn | P | S | Cr | Ni | Mo | Nb | N |
|-----|-------|-------|-----|-----|------|-----|-----|------|----|
| ± 0 | + 0.3 | - 0.5 | ± 0 | ± 0 | -0.7 | ± 0 | ± 0 | -0.1 | ±0 |

As can be seen, the losses of alloying elements in the slag reaction are very small and the pick-up of undesired elements is equal to nil. The transfer of individual alloying elements through the molten slag pool from the strip electrodes end to an undiluted weld metal can also be expressed in the following manner:

- Carbon 100%
- Manganese 80 %
- Chromium 97 %
- Nickel 100 %
- Niobium 90 %

These fluxes contain very low siliceous oxide. The consequence is that the deposited metal are obtained with extremely low oxygen concentration and a high degree of cleanliness in terms of level and size of non-metallic inclusions. The metal transfer through the molten slag pool from the strip to the deposited is expressed as alloying vectors. It has also observed that in order to keep the process within stable electroslag operating conditions the fluxes may contain only small amount of metallic elements such as Cr, Ni, and Mo.

2.3.10.2.5 Handling of the Flux:

All fluxes are slightly hygroscopic and any moisture pick-up will change the physical and chemical properties which may lead to defect in the weld deposit. It is recommended that damp fluxes are re-baked before use in the temperature ranges 250⁰ C for 1- 2 hours. Certain fluxes can be recycled during the welding operation. It is recommended that recycled and new flux is mixed in the ratio upto 2:1.

2.3.10.2.6 Flux Consumption:

The varies widely depending on the flux handling system used during the welding operation and to a certain extent, on the welding parameters. In case a flux recovery unit is used during the welding operation, the flux consumption is in the order of 8.0- 1 weight unit flux per weight unit strip electrode for the ESSC process.

2.3.10.2.7 Depth of Flux Burden:

As a general rule, the depth of the flux should be between 0 and 5 mm more than the length of the electrode extension. With a greater flux burden, the rate of dilution and flux consumption will increase slightly. Furthermore, the radiation from the visible molten slag pool is somewhat reduced, as is also the tendency toward slag spatter. The latter should be controlled by a proper setting of welding current and voltage.

2.3.11 Thermal History of ESSC process**2.3.11.1 Preheat and Interpass Temperatures**

Generally, preheating is not recommended immediately prior to welding as it may negatively affect cooling rates required to achieve optimal phase balance. The maximum recommended interpass temperature should not exceed 200°C (392°F) for DSS alloys and 150°C (302°F) for SDSS alloys throughout cladding operations. Excessive interpass temperatures can cause embrittlement. In these situations, harmful phases could form over prolonged time.[39].

2.3.11.2 Heat Input

The energy input per unit surface of weld deposit, Q_p , for different surfacing system like ESSC, SASC etc. can be expressed as,

$$Q_p = \frac{IV}{SW} \times 60 \text{ J/Surface unit}$$

Where,

I = Welding current (A)

V = Voltage (V)

S = welding speed (mm/min or in/min)

W = Width of bead (mm or in.)

Heat input other than surfacing systems can be expressed as,

$$Q_p = \frac{IV}{S} \times 60 \text{ J/mm}$$

This energy is consumed for fusion of the strip electrode and flux, Penetration of parent metal, heating of the surrounding metal, will cause structural changes in parent metal which may change its property.

2.4 Effect of Alloying Addition in Austenitic stainless steel:

2.4.1 Effect of Chromium Addition in Austenitic stainless steel:

Chromium and Nickel in adequate amounts are primarily responsible for the stabilization of the austenite phase relative to the ferrite phase. Both elements contribute to corrosion resistance. It provide corrosion protection oxidizing environments (nitric acid) by forming $(Fe,Cr)_2O_3$ oxide film. Presence of Cr increases the stability of oxide film as it has high affinity toward O_2 . For adequate corrosion resistance in most media, Cr content should exceed 13%. It strong ferrite stabilizer & also strong carbide former and mainly formed common carbide $M_{23}C_6$ (M=some fraction of Fe or Mo). It also forms Cr_2N mainly in ferritic & duplex stainless steel.

2.4.2 Effect of Nickel Addition in Austenitic stainless steel:

It is strong austenite forming element. It provides corrosion protection mainly in reducing environments such as sulphuric acid. It is Good solid solution strengthening ability & improve toughness for martensitic & ferritic SS. When it is added up to 2% Ni in high Cr- ferritic steel it decreases the ductile to brittle transition temperature. Great advantage of addition Ni in stainless steel is that it is not carbide former & not inter-metallic compound former which reduced the tendency toward sigma phase formation.

2.4.3 Effect of Carbon and Carbides in Austenitic stainless steel:

Carbon in solution has a strengthening effect on the austenite structure. For this reason, many specifications for elevated temperature applications, where retention of static strength and measured creep strength are important, require a higher minimum limit for carbon. But during welding if base metal has $> 0.03\%$ carbon it will fore $Cr_{23}C_6$ precipitation which lead to sensitization. So carbon should be $<0.03\%$ or addition of strong carbide forming element such as Nb, Ti to reduce tendency toward IGC. [40].

2.4.4 Effect of Nitrogen Addition in Austenitic stainless steel:

Like carbon, nitrogen is an interstitial solute in the austenite matrix of stainless steels. It also strengthens the alloy through the considerable strain imparted to the lattice when it takes up interstitial sites. As an austenite former, nitrogen has a nickel equivalency of 30, making it as, or nearly as, potent as carbon. By using additions of 3% or more nitrogen to the argon shielding gas for gas tungsten arc welds of 308L, the nitrogen level to increase to over 0.2% and the ferrite number to drop from 21 to under 5.

In 0.15% nitrogen steel, as little as 0.07% niobium caused the formation of a finely divided CrNbN precipitate during annealing and stabilizing heat treatments. This has the effect of retarding the intergranular precipitation of chromium carbides by a preferential precipitation of the carbide at the CrNbN precipitate. A high dislocation density occurs surrounding the CrNbN precipitate, which provides trapping sites for carbide precipitation, thus reducing grain boundary precipitation and consequent intergranular corrosion. In a study of stainless steels for cryogenic temperature use, the advantage of nitrogen additions to non-niobium containing alloys, but observe that “due to the precipitation of nitrides or carbonitrides of Nb, nitrogen is of limited use in stabilizing the austenite phase in weldable steels 347.” It would be well to avoid placing too much emphasis on the similarity of nitrogen effect in Type 347 steel, because Nb form nitrides of distinctly different stability [41].

2.4.5 Effect of Molybdenum addition in Austenitic stainless steel:

Molybdenum acts to support chromium in providing pitting corrosion resistance to stainless steels. When the chromium content of a stainless steel is at least 18%, additions of molybdenum become about three times as effective as chromium additions against pitting and crevice corrosion in chloride-containing environments. Molybdenum is a ferrite former and also increases the tendency of a stainless steel to form detrimental intermetallic phases. Therefore, it is usually restricted to less than about 7.5% in austenitic stainless steels

2.4.6 Effect of Niobium Addition in Austenitic stainless steel:

Austenitic stainless steels are the most popular metallic materials because of their relatively low cost, ease of fabrication and reasonable corrosion resistance . One of the main disadvantages of stainless steels is the problem of localized corrosion when they are exposed to chloride solutions. There are several surface modification techniques to improve stainless steels' behavior against localized corrosion in such media. One of them is addition of alloying elements such as Mo, Ni, V, Si. Niobium is a ferrite forming element. It is half as effective as chromium, assigning a coefficient of 0.5. The principal purpose of niobium is to form carbide preferentially to that of chromium carbide. This has the effect of reducing the free carbon in the alloy to a level below which chromium carbides do not precipitate in grain boundaries, thus avoiding depletion of the region of

chromium and avoiding intergranular corrosion. In order to be fully effective, the steel should be given a stabilizing heat treatment at temperatures between 850°C and 1100°C. The niobium carbides, however, will redissolve at higher temperatures, and uniformly distributed within the grains. Niobium strengthens the stainless steel in two ways, as a solid solution hardener and as a precipitation hardener in the form of NbC, NbN, CrNbN and Fe₂Nb. Nb enhances the mechanical properties at high temperatures in austenitic stainless steel. The presence of Nb increases the proof strength of austenitic stainless steels even at high temperatures. Researcher Mr. *Abdel Salam Hamd* has investigated the corrosion behavior of austenitic stainless steel specimens containing different amount of Nb alloying element using electrochemical impedance spectroscopy (EIS) in 3.5% NaCl. It shows that surface resistance of with 1.24 Nb sample were better as come to 0 % Nb & 1.14 % Nb samples. This is because of the amount of surface defects were decreases by increasing the amount of Nb in stainless steel. The polarization study in 3.5 % NaCl solution shows that the formation of Nb rich protective oxide film shifts the current to more noble one and consequently, reducing the number of pits [42].

2.5 Solidification Mode of Austenitic Stainless Steel Weld Metals

There are four solidification mode & solid state transformation possibilities for austenitic stainless steel weld metals as follows.

- A-austenitic
- AF -austenitic–ferritic or primary austenitic
- FA- ferritic-austenitic or primary ferritic
- F -ferritic

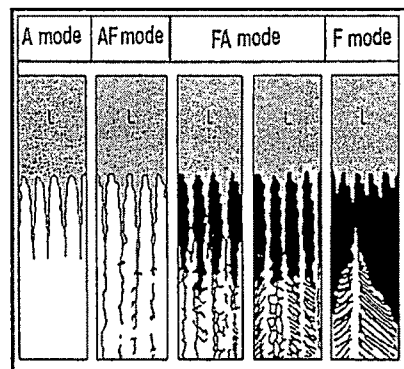
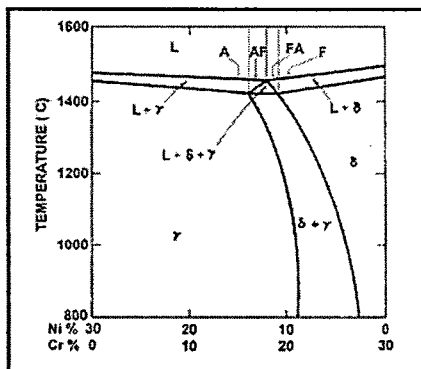


Fig. 2.20 Ternary diagram of Fe-Cr-Ni system with mode of solidification

Fig. 2.21 Mode of solidification with ferrite morphology

Fig 2.20 shows the ternary diagram of Fe-Cr-Ni system with mode of solidification & Fig.2.21 shows the various mode of solidification with different ferrite morphology.

Various solidification mode can be predicted in terms of ratio of Cr equivalent & Ni equivalent values

$$C_{req} = Cr + 1.37Mo + C + 1.5Si + 2Nb + 3Ti \dots\dots\dots(1)$$

$$N_{ieq} = Ni + 0.31Mn + 22C + 14.2N + Cu \dots\dots\dots(2)$$

If C_{req}/N_{ieq} ratio is low- A-mode solidification occurs while C_{req}/N_{ieq} ratio is high- AF,FA,F-mode solidification occurs & Transition from AF to FA mode occurs when the C_{req} / N_{ieq} ratio of 1.55

2.5.1 A Mode solidification

This is defined as Type A solidification because when solidification occur as primary austenitic & it will remain austenite upon cooling to room temperature. Primary phase is austenite due to segregation of alloying elements & impurities elements & relatively low diffusivity of this element at elevated temperature. Alloy such as Type 304 & 316 solidify as type A & showing cell & dendrites solidification substructure in Fig.2.22.

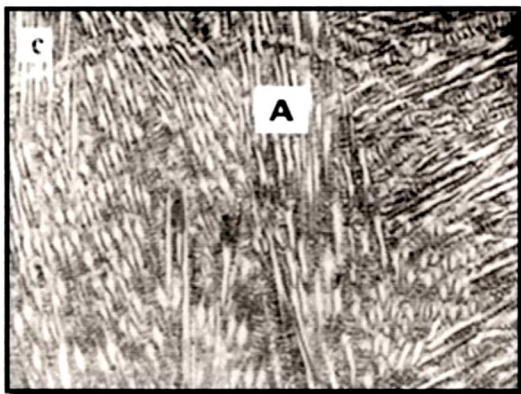


Fig. 2.22 316L weld metal with 0.14% N

2.5.2 AF- Mode solidification

If some ferrite is form at end of primary austenite solidification via eutectic reaction, solidification is termed Type AF. This occur if sufficient ferrite promoting element (Cr & Mo) partition to the solidification sub-grain boundaries during solidification to promote formation of ferrite as terminal solidification product. Once ferrite is form it remain stable

& resist transformation to austenite during welding since it is already enriched in ferrite-promoting elements.

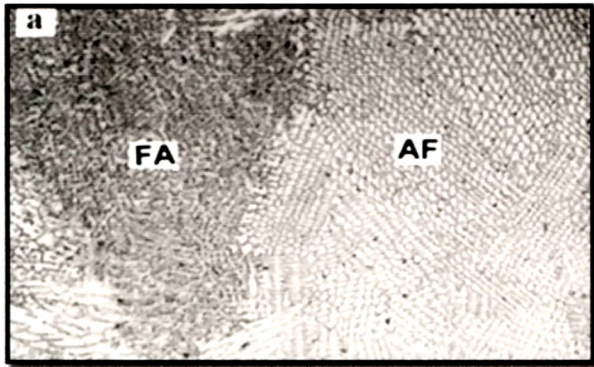


Fig. 2.23 316L weld metal without any N addition showing AF mode

2.5.3 FA- Mode solidification

When solidification occurs as primary ferrite there are two possibilities. If some austenite forms at the end of solidification is term as Type FA. This austenite form via peritectic - eutectic reaction & exits at ferrite solidification boundaries at the end of solidification. When solidification completed, the microstructure would be primary ferrite + inter dendrite of austenite.

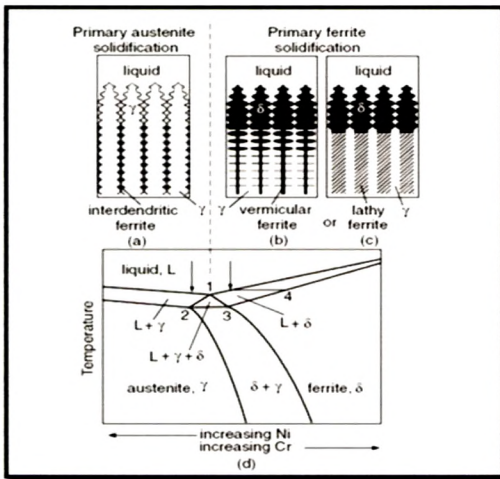


Fig.2.24 Relationship of solidification type to the pseudo binary diagram



Fig, 2.25 FA mode weld metal in 312 austenitic stainless steel

Amount of austenite is depending on solidification condition and Ni_{eq}/Cr_{eq} value. As ratio of Ni_{eq}/Cr_{eq} increased amount of Austenite is decrease until solidification is entirely ferritic . At this point yhe solidification type shift to FA to F. Weld metal

cooling rate moderate & Ratio Ni_{eq}/Cr_{eq} is low within the FA range, vermicular or skeletal morphology due to austenite consuming ferrite until ferrite sufficiently enriched in ferrite promoting element (Cr & Mo) while Weld metal cooling rate high & Ratio Ni_{eq}/Cr_{eq} is increase within FA range, lathy ferrite morphology due to restricted diffusion during the ferrite to austenite transformation.

2.5.4 F- Mode solidification

If solidification occurs completely as ferrite, it is termed as Type F. In this case microstructure is fully ferritic at the end of solidification. As shown in fig. 2.24, when weld metal cool below ferrite solvus than austenite form within the microstructure first at the ferrite grain boundaries. Because the structure was fully ferritic in the solid state between the solidus & ferrite solvus, diffusion of ferrite is eliminated at most of all composition gradient resulting fully ferrite at end of solidification and thus when the transformation starts, the microstructure consists of large relatively homogeneous ferrite grains. The degree of transformation of austenite is depend on cooling rate and Ni_{eq}/Cr_{eq} value. At low Cr_{eq}/Ni_{eq} value within F range the transformation begins at a High temperature & at low to moderate weld cooling rate this will cause ferrite will transform into austenite while at high cooling rate diffusion of ferrite is suppressed and austenite not consume ferrite. Similarly At higher Cr_{eq}/Ni_{eq} value, value within F range ferrite solvus depressed and transformation will occur at low temperature lead to high ferrite content. The microstructure of Type S solidification in austenitic stainless steel again is function of composition & cooling rate. At low Cr_{eq}/Ni_{eq} value within F range acicular ferrite structure is formed within the ferrite grain & at high Cr_{eq}/Ni_{eq} value, value within F range ferrite matrix with grain boundaries austenite and Widmanstätten austenite plates that nucleate at the grain boundary austenite or within the ferrite grains[43].

2.6 Ferrite Content in Austenitic Claddings

To be resistant against hot cracking, the austenitic standard strip electrodes are alloyed to produce a weld metal containing a certain amount of δ - Ferrite. Frequently the content of δ -ferrite is limited by the rules of the chemical and petrochemical industry to maximum of 8% (or to be between 2 and 8%). With higher a concentration a ferritic lattice at the grain boundaries may occur, which impairs the corrosion resistance and the ductility of

cooling rate moderate & Ratio Ni_{eq}/Cr_{eq} is low within the FA range, vermicular or skeletal morphology due to austenite consuming ferrite until ferrite sufficiently enriched in ferrite promoting element (Cr & Mo) while Weld metal cooling rate high & Ratio Ni_{eq}/Cr_{eq} is increase within FA range, lathy ferrite morphology due to restricted diffusion during the ferrite to austenite transformation.

2.5.4 F- Mode solidification

If solidification occurs completely as ferrite, it is termed as Type F. In this case microstructure is fully ferritic at the end of solidification. As shown in fig. 2.24, when weld metal cool below ferrite solvus than austenite form within the microstructure first at the ferrite grain boundaries. Because the structure was fully ferritic in the solid state between the solidus & ferrite solvus, diffusion of ferrite is eliminated at most of all composition gradient resulting fully ferrite at end of solidification and thus when the transformation starts, the microstructure consists of large relatively homogeneous ferrite grains. The degree of transformation of austenite is depend on cooling rate and Ni_{eq}/Cr_{eq} value. At low Cr_{eq}/Ni_{eq} value within F range the transformation begins at a High temperature & at low to moderate weld cooling rate this will cause ferrite will transform into austenite while at high cooling rate diffusion of ferrite is suppressed and austenite not consume ferrite. Similarly At higher Cr_{eq}/Ni_{eq} value, value within F range ferrite solvus depressed and transformation will occur at low temperature lead to high ferrite content. The microstructure of Type S solidification in austenitic stainless steel again is function of composition & cooling rate. At low Cr_{eq}/Ni_{eq} value within F range acicular ferrite structure is formed within the ferrite grain & at high Cr_{eq}/Ni_{eq} value, value within F range ferrite matrix with grain boundaries austenite and Widmanstatten austenite plates that nucleate at the grain boundary austenite or within the ferrite grains[43].

2.6 Ferrite Content in Austenitic Stainless Steel Claddings

To be resistant against hot cracking, the austenitic standard strip electrodes are alloyed to produce a weld metal containing a certain amount of δ - Ferrite. Frequently the content of δ -ferrite is limited by the rules of the chemical and petrochemical industry to maximum of 8% (or to be between 2 and 8%). With higher a concentration a ferritic lattice at the grain boundaries may occur, which impairs the corrosion resistance and the ductility of

the welded overlay. At higher operating temperatures or during the post weld heat treatment (as required by the European pressure vessel and ASME-codes), Carbides can precipitate to the ferritic lattice and sigma phase will be found. Sigma phase mainly lowers the toughness and can lead to inter-granular corrosion. Consequently the adjustment of the δ -ferrite content in the weld metal is of most importance. The biggest influence on the resulting ferrite content greatly involves welding speed, which also affects the dilution of the base material. If a very low travel speed is used with overlaid strip during cladding of the first layer, the result would be a very low dilution but at the same time acquiring an unacceptable high content of ferrite. Welding speed is not only an economical factor but also a metallurgical one. With strip electrodes like OK Band 11.71, 11.72 and 11.73 / 60x0,5 mm for electroslog cladding, welding speeds of 18 to 20 cm/min are selected as usual parameters (about 1,200 Amps and 24 Volts). If the requested thickness of the overlay is more than 5 mm, a second layer with another strip (OK Band 11.61, 11.62 or 11.63) is recommended instead of cladding a single thick layer with high ferrite content [44].

2.7 Post Weld Heat Treatment of Weld Overlays

Post weld heat treatment (PWHT), defined as any heat treatment after welding, is often used to improve the properties of a weldment. In concept, PWHT can encompass many different potential treatments; however, in steel fabrication, the two most common procedures used are post heating and stress relieving.

2.7.1 Post Heating

Post heating is used to minimize the potential for hydrogen induced cracking which may occur due to a sensitive base metal microstructure, high levels of hydrogen, and/or high level of stress. In ferritic steels, hydrogen embrittlement only occurs at temperatures close to the ambient temperature. Therefore, it is possible to avoid cracking in a susceptible microstructure by diffusing hydrogen from the welded area before it cools. After welding has been completed, the steel must not be allowed to cool to room temperature; instead, it should be immediately heated from the interpass temperature to the post heat temperature and held at this temperature for some minimum amount of time. However, when the

causes of hydrogen cracking are not present, post heating is not necessary, and unjustifiable costs may result if it is done. Although various code and service requirements can dictate a variety of temperatures and hold times, 450°F(230°C) is a common post heating temperature to be maintained for 1 hour per inch (25 mm) of thickness.

2.7.2 Stress Relieving

Stress relief heat treatment is used to reduce the stresses that remain locked in a structure as a consequence of manufacturing processes. There are many sources of residual stresses, and those due to welding are of a magnitude roughly equal to the yield strength of the base material. Uniformly heating a structure to a sufficiently high temperature, but below the lower transformation temperature range, and then uniformly cooling it, can relax these residual stresses. Carbon steels are typically held at 600 to 675°C for 1 hour per inch (25 mm) of thickness. Stress relieving offers several benefits. For example, when a component with high residual stresses is machined, the material tends to move during the metal removal operation as the stresses are redistributed. After stress relieving, however, greater dimensional stability is maintained during machining, providing for increased dimensional reliability. In addition, the potential for stress corrosion cracking is reduced, and the metallurgical structure can be improved through stress relieving. The steel becomes softer and more ductile through the precipitation of iron carbide at temperatures associated with stress relieving. At the elevated temperatures associated with stress relieving, hydrogen often will migrate from the weld metal and the heat affected zone. However, HIC can be minimized by heating at temperatures lower than stress relieving temperatures, resulting in lower PWHT costs[45].

2.7.3 Effect of Post weld heat treated on microstructures of weld overlay:

Large pressure vessels are used in hydrogen containing environments, for example, in the petroleum industry in hydrocracking, hydrodesulphurisation and catalytic reforming are operated at high temperatures(450°C)and at high hydrogen partial pressures(15 MPa). The vessels are generally fabricated from low alloy creep resistant steels. In addition to operational stresses, they experience thermal stresses during manufacturing and service, because of the different thermal conductivities and expansion coefficients of stainless

steel and low carbon low alloy steel [46]. In the weld overlay of austenitic Stainless steel at least 5%, by volume of delta ferrite in the microstructure is required to minimize the thermal cracking during the weld overlay solidification. On the other hand, the ductility of the weld overlay is reduced when the delta ferrite content is higher than 10%. Post-weld heat treatment (PWHT), is used to decrease residual stress levels, improve the ductility, increase the Intergranular corrosion resistance of weld overlay [47]. However, during PWHT, carbon diffuses from the low steel to the austenitic weld overlay generating a decarburised layer in the low alloy steel adjacent to the interface and a carbon-enriched layer in the nearby weld overlay. Most of the carbon in the carbon-enriched zone precipitates as carbides, thereby decreasing the dissolved Cr concentration in the matrix. These micro structural changes, which depend on the PWHT temperature and duration and on the chemical composition of the two metals, cause changes in mechanical properties. Phase transformation or precipitation of carbides may occur in the metastable austenite/ferrite weld overlay during PWHT process. The formation of intermetallic compounds during PWHT may affect the pitting corrosion behavior [46].

During postweld heat treatment for 16 h at 700⁰ C, several diffusion-based reactions occur in the cladded joint, especially at and near the weld interface. Fig.2.26 is a micrograph of the interface region after PWHT in the single-layer overlay. It shows a heavily dark-etching layer marking the transition zone between the base metal and bulk weld metal. This was the region which exhibited a martensitic structure in the as-welded condition and in which considerable carbide precipitation has occurred during PWHT. Next to this layer on the clad metal side is a region of weld metal showing the total absence of ferrite. This fully austenitic region is bounded on the other side by a grain boundary running approximately parallel to the dark-etching layer and the weld interface. This grain boundary has been referred to in the literature as a 'Type II boundary' [48, 49]. Further into the weld metal on the left of the Type II boundary is the more usual austenitic weld metal structure containing ferrite in the substructure boundaries within the austenite grains. The boundaries of these austenite grains represent the conventional or Type I grain boundaries.

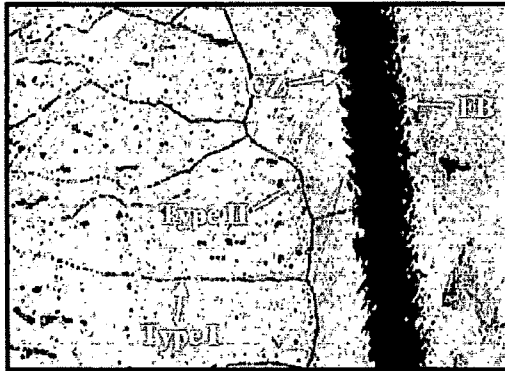


Fig.2.26. Weld interface in single-layer cladding after PWHT, Etchant : Aquaregia, 400X
 Note the presence of a carburized zone and Type II grain boundary. Type I and Type II grain boundaries are indicated by arrows.



Fig.2.27 Base metal region adjoining weld interface after PWHT in single-layer cladding. Etchant: Nital, 200X
 Note the presence of a decarburized, coarse ferritic region(DZ) .

In Fig. 2.27 on the base metal side of the dark-etching interface layer exhibits a nearly totally decarburized base metal structure. Note also that the ferrite grains here are able to grow to large sizes in the absence of the carbide phase. Carbon in this region has diffused from the base metal toward the overlay because of the concentration gradient and its affinity for the higher Cr content in the clad metal.

2.7.4 Effect of PWHT on Microhardness

The microhardness distributions across the weld interface both in the as-welded condition and after PWHT are plotted in Fig.2.28.

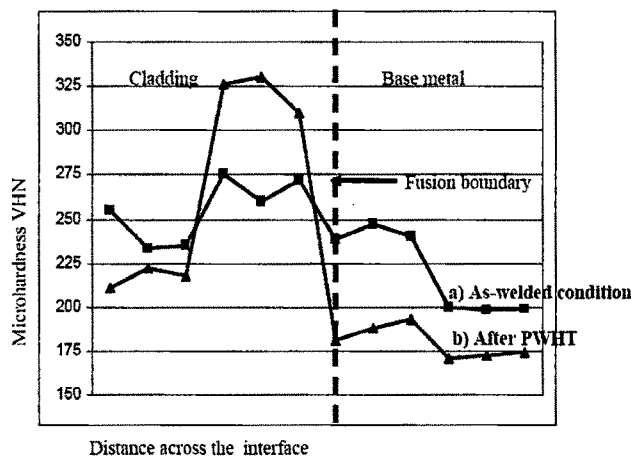


Fig. 2.28 : Microhardness distributions across clad interface

In the as-welded condition, there is a moderate increase in hardness at the weld interface region, which can be attributed to the formation of a low-carbon martensite. After postweld heat treatment the hardness of this region registers a significant increase, presumably as a result of heavy carbide precipitation. On the base metal side of the interface after postweld heat treatment, there is a noticeable softening effect as a result of the migration of carbon from this region to the interface.

2.7.4.1 Composition gradients

The chemical analyses of the bulk weld metal in the single-layer overlay at 2.5 mm, 3 mm and mm from the fusion boundary are given in Table 2.5 . These show a relatively uniform composition in the bulk cladding, corresponding to the strip electrode mixed with the base metal to an average degree of dilution depending on the welding parameters. However, as the base metal is approached, there are steep concentration gradients in the interface region that includes the transition zone described above. Scanning electron microscopy EDS analyses of the interface region both in the as-welded and postweld heat treated condition are listed in Table 2.6 [50].

Table 2.5: Chemical analysis of single-layer overlay in the bulk weld metal

| Elements | Location From Fusion Line to Overlay (wt.%) | | |
|------------|---|--------|--------|
| | 2.5 mm | 3.0 mm | 3.5 mm |
| Carbon | 0.022 | 0.022 | 0.024 |
| Manganese | 1.11 | 1.01 | 1.01 |
| Silicon | 0.28 | 0.2 | 0.192 |
| Chromium | 18.11 | 18.14 | 18.56 |
| Molybdenum | 0.17 | 0.2 | 0.17 |
| Nickel | 9.34 | 9.53 | 9.46 |
| Niobium | 0.32 | 0.35 | 0.34 |

Table 2.6 : EDS (SEM) chemical analysis in the interface transition zone in single-layer overlay

| Description | %Cr | %Ni |
|------------------------|-------|------|
| As-welded, location 1 | 3.23 | 1.61 |
| As-welded, location 2 | 3.51 | 1.42 |
| After PWHT, location 1 | 13.44 | 5.17 |
| After PWHT, location 2 | 11.66 | 4.02 |

Double PWHT procedures have been developed to significantly decrease the hardness of the interface region of claddings, compared to the hardness measured after a single PWHT. With a tempering in two steps lower hardness values are to be found, compared to a single PWHT due to annealing of the fresh martensite formed during cooling.

2.8 Testing & Evaluation weld overlays

2.8.1 Ferrite Content Determination:

The ferrite content in stainless steel weld metals plays an important role in determining the fabrication and service performance of a welded construction. The most important beneficial effect of ferrite in nominally austenitic stainless steel weldments is the well-established relationship between a reduced sensitivity to hot cracking and the presence of a certain amount of ferrite in the deposited metal. The minimum ferrite limit necessary to assure freedom from cracking depends, among other factors, on the weld metal composition. The upper limit results from possible impairment of either mechanical or corrosion resisting properties, or both, according to service conditions [51]. Ferrite content can be determined by metallographic technique but it has disadvantage like it is destructive, time consuming & reproducibility of microstructure required more skilled. For these reason, magnetic technique have been widely adopted. These technique take advantage of the fact that ferrite is ferromagnetic at room temperature, while austenite is not.

2.8.1.1 Instruments for ferrite content measurements:

MagneGage instruments: It involved relating force required to pull a small magnet from the weld surface (tearing force) to the ferrite content.

Fischer Feritscope MP 30: This technique use eddy current probe to measure ferrite content. Such instrument can only Calibrated with secondary weld metal standards but produce results identical to those obtained with MagneGang. It is measured the ferrite content in a range of 0.1 to 110 FN or 0.1 to 80% FE in austenitic and duplex steel. when probe contact the test object it provide acoustical signal which give automatic measurement of ferrite content[52].

2.8.2 Micro-hardness testing of Weld overlays

2.8.2.1 Vickers Hardness Test

The Vickers hardness test operates on similar principles to the Brinell test, the major difference being the use of a square based pyramidal diamond indenter rather than a hardened steel ball. Also, unlike the Brinell test, the depth of the impression does not affect the accuracy of the reading so the P/D^2 ratio is not important. The diamond does not deform at high loads so the results on very hard materials are more reliable. The load may range from 1 to 120kgf and is applied for between 10 and 15 seconds.

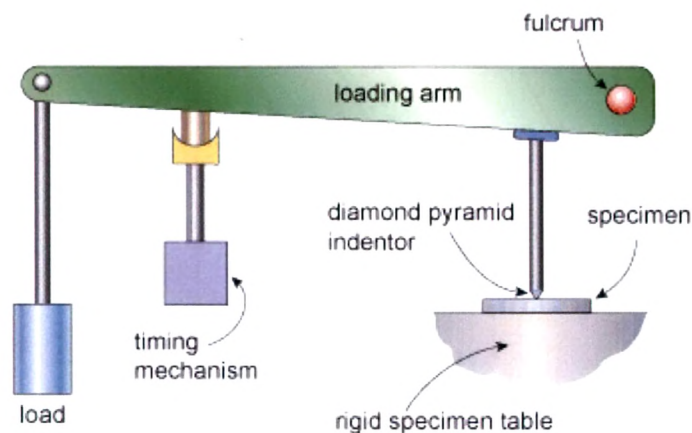


Fig.2.29 Schematic principles of operation of Vickers hardness machine

The basic principles of operation of the Vickers hardness test are illustrated in Fig.2.29 where it can be seen that the load is applied to the indenter by a simple weighted lever. In older machines an oil filled dash pot is used as a timing mechanism - on more modern equipment this is done electronically

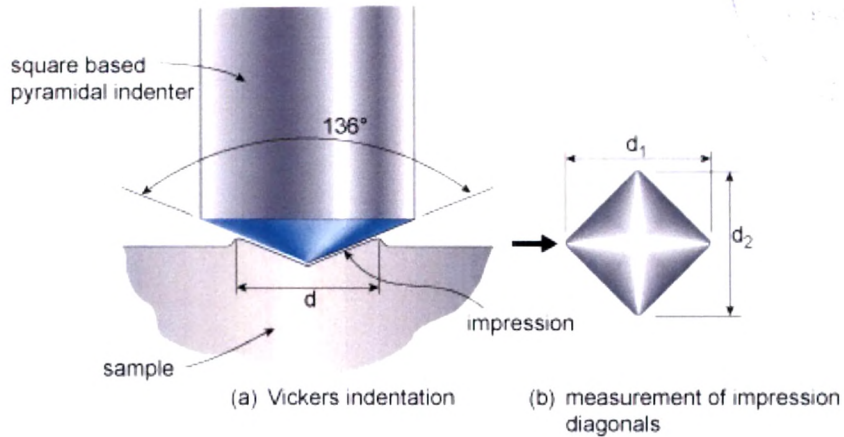


Fig. 2.30 Detail of indentation

As illustrated in Fig.2.30(b) two diagonals, d_1 and d_2 , are measured, averaged and the surface area calculated then divided into the load applied. As with the Brinell test the diagonal measurement is converted to a hardness figure by referring to a set of tables. The hardness may be reported as Vickers Hardness number (VHN), Diamond Pyramid Number (DPN) or, most commonly, Hv_{xx} where 'xx' represents the load used during the test[53]. The Vickers hardness value (VHN) can be calculated from the applied load divided by areas of indentation, at which the latter is derived from the diagonals of the pyramid as expressed in the equation below

$$VHN = \frac{2P \sin(\theta/2)}{d^2} = \frac{1.854P}{d^2}$$

Where ,

P = the applied load, kg

d = the average length of the diagonals = $(d_1 + d_2)/2$, mm

θ = angle between the opposite faces of the diamond = 136°

2.8.3 Metallographic Analysis of Weld overlays

It is the study of the physical structure and components of metals, typically using microscopy. The surface of a metallographic specimen is prepared by various methods of grinding, polishing, and etching. After preparation, it is often analyzed using optical or electron microscopy. Using only metallographic techniques, a skilled technician can identify alloys and material properties[54].

Table-2.7 List of Etchant for various alloys

| Sr. No | Etchant Name | Composition | Methods | Type of Alloy |
|--------|-----------------------|--|--|---|
| 1 | Nital (2%) | 2cc HNO ₃ + 98cc Ethyl alcohol | Immersion | Caron steel, Low alloy steel |
| 2 | Pical (5%) | 5gr Picric acid + 100cc Ethyl alcohol | Immersion | Caron steel, Low alloy steel |
| 3 | Oxalic acid | 10gr oxalic acid + 10cc H ₂ O | Electrolytic at 200/400 Ma. | 304, 304L, 309, 310, 316, 347, 304, 304L, 309, 310, 316, 347, |
| 4 | Viella's | 5cc HCl + 2gr Picric acid + 100cc Ethyl alcohol | Immersion or Swab | 304, 304L, 309, 310, 316, 347, 440A, 440B, 440C |
| 5 | Aqua Regia in alcohol | 100cc HCl + 3cc HNO ₃ + 100cc Methyl alcohol | Immersion | 304, 304L, 309, 310, 316, 347, |
| 6 | Chromic acid | 10gr CrO ₃ + H ₂ O | Electrolytic at 200/400 Ma. | 304, 304L, 309, 310, 316, 347, |
| 7 | Glyceregia | 15cc HCl + 10cc Glycerol + 5cc HNO ₃ | Use Fresh - Under Hood - Swab - Do Not Store | 304, 304L, 309, 310, 316, 347, 440A, 440B, 440C, 416, 430F, 446 |
| 8 | Ralph's | 100cc H ₂ O + 200cc methyl alcohol + 100cc HCl + 2gr CuCl ₂ + 7gr FeCl ₂ + 5cc HNO ₃ | Swab | 304, 304L, 309, 310, 316, 347, 416, 430F, 446 |

2.8.3.1 Analysis techniques

Many different microscopy techniques are used in metallographic analysis. Prepared specimens should be examined with the unaided eye after etching to detect any visible areas that have responded to the etchant differently from the norm as a guide to where micro-structural examination should be employed. Light optical microscopy (LOM) examination should always be performed prior to any electron metallographic (EM) technique, as these are more time-consuming to perform and the instruments are much more expensive. But, morphology of inter-metallic compound and precipitation product can be observed under SEM as magnifications about 2000 to 3000X is required.

2.8.3.2 SEM & EDAX Analysis

2.8.3.2.1 Scanning Electron Microscope (SEM) Study:

A scanning electron microscope (SEM) produces images of a sample by scanning it with a focused beam of electrons. The electrons interact with electrons in the sample, producing various signals that can be detected and that contain information about the sample's surface topography and composition. The electron beam is generally scanned in a raster scan pattern, and the beam's position is combined with the detected signal to produce an image. SEM can achieve resolution better than 1 nanometer. Specimens can be observed in high vacuum, low vacuum and in environmental SEM specimens can be observed in wet conditions.

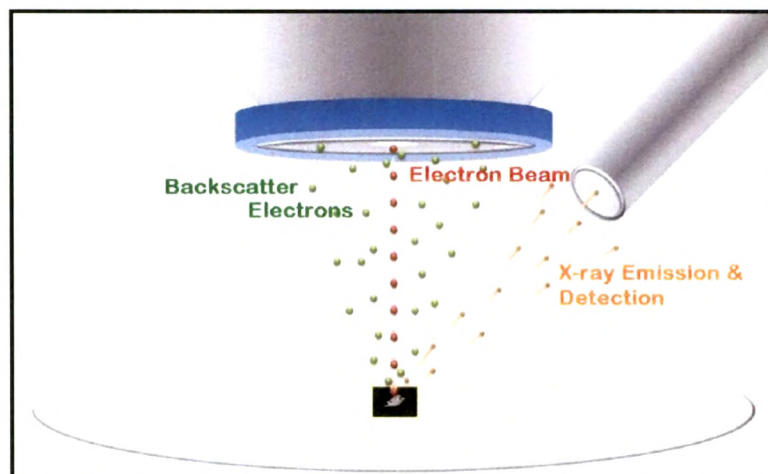


Fig 2.31: Principle & working of SEM

Fig.2.31 shows the principle & working of SEM. The types of signals produced by a SEM include secondary electrons (SE), back-scattered electrons (BSE), characteristic X-rays, light (cathodoluminescence) (CL), specimen current and transmitted electrons. A wide range of magnifications is possible, from about 10 times (about equivalent to that of a powerful hand-lens) to more than 500,000 times, about 250 times the magnification limit of the best light microscopes. Back-scattered electrons (BSE) are beam electrons that are reflected from the sample by elastic scattering. BSE are often used in analytical SEM along with the spectra made from the characteristic X-rays, because the intensity of the BSE signal is strongly related to the atomic number (Z) of the specimen. BSE images can provide information about the distribution of different elements in the sample. For the

same reason, BSE imaging can image colloidal gold immuno-labels of 5 or 10 nm diameters, which would otherwise be difficult or impossible to detect in secondary electron images in biological specimens. Characteristic X-rays are emitted when the electron beam removes an inner shell electron from the sample, causing a higher-energy electron to fill the shell and release energy. These characteristic X-rays are used to identify the composition and measure the abundance of elements in the sample.

2.8.3.2.2 Energy Dispersive X-ray (EDAX):

Energy-dispersive X-ray spectroscopy (EDS, EDX, or XEDS) is an analytical technique used for the elemental analysis or chemical characterization of a sample. It relies on the investigation of an interaction of some source of X-ray excitation and a sample.

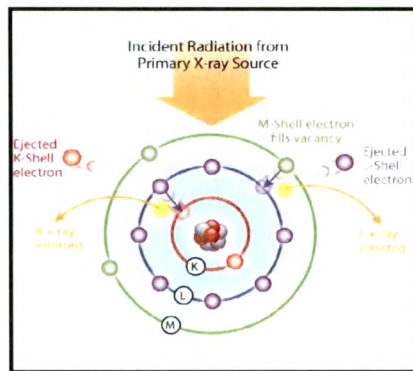


Fig. 2.32 Principle of EDAX Analysis

Its characterization capabilities are due in large part to the fundamental principle that each element has a unique atomic structure allowing unique set of peaks on its X-ray spectrum. To stimulate the emission of characteristic X-rays from a specimen, a high-energy beam of charged particles such as electrons or protons, or a beam of X-rays, is focused into the sample being studied. At rest, an atom within the sample contains ground state (or unexcited) electrons in discrete energy levels or electron shells bound to the nucleus. The incident beam may excite an electron in an inner shell, ejecting it from the shell while creating an electron hole where the electron was. An electron from an outer, higher-energy shell then fills the hole, and the difference in energy between the higher-energy shell and the lower energy shell may be released in the form of an X-ray. The number and energy of the X-rays emitted from a specimen can be measured by an energy-dispersive spectrometer. As the energy of the X-rays is characteristic of the difference in energy

between the two shells, and of the atomic structure of the element from which they were emitted, this allows the elemental composition of the specimen to be measured.

2.8.4 Corrosion Rate Measurement of weld overlays

Corrosion measurement is the quantitative method by which the effectiveness of corrosion control and prevention techniques can be evaluated and provides feedback to enable corrosion control and prevention methods to be optimized. It is meant to predict compatibility of a material before it is used in an environment and to aid in understanding why a material-environmental interaction could occur. Corrosion measurement could employ a variety of techniques to determine the corrosiveness of the environment and the extent of metal loss. These techniques can be broadly classified as destructive or non-destructive. A measurement is said to be destructive if it alters the corrosion process during the measuring process (e.g. potentiodynamic polarization) or if the material is physically removed from the environment (e.g. weight loss measurement). Non-destructive techniques, including linear polarization resistance, electrochemical impedance spectroscopy, and electrochemical noise, could be used to make repeated measurements at different time intervals. For the purpose of this study, the destructive evaluation technique is briefly reviewed.

2.8.4.1 Weight loss technique

The weight loss technique which involves exposing a specimen of material to the corroding environment for a given duration and then removing the specimen for weighing is the best known and the simplest of all corrosion measurement techniques. The weight loss or gain is taken over the period of exposure, and later expressed as a corrosion rate. The advantage of the weight loss technique is that the corrosion which has actually occurred can be observed on the sample. Moreover, this technique allows a visual examination, physical measurements and the chemical analysis of the corrosion products. Uniform corrosion takes place over the entire surface of the coupon, the corrosion rate is calculated from the weight loss, time of exposure and original exposed surface area of the material by the following formula

$$\text{mpy} = \frac{534W}{DAT}$$

Where:

mpy = mils per year

W = weight loss, mg

A = area of specimen, in²

t = exposure time, hr

D = density of specimen, g/cm³

2.8.4.2 Electrochemical techniques

Aqueous corrosion reactions are electrochemical in nature; therefore, they can be easily studied using electrochemical techniques. Electrochemical techniques could provide a feasible alternative for rapid prediction or evaluation of alloy corrosion. It could be done to predict corrosion of a material in a plant operation or in the laboratory and its application in evaluating alloy corrosion arises from its relative ease of implementation requiring instrumentation that is comparatively economical while being completely mechanized. A large number of electrochemical techniques used for corrosion measurements exist. These include, amongst others, open circuit potential measurement, potentiodynamic polarization, cyclic potentiodynamic polarization scans (especially for predicting localized corrosion), linear polarization resistance, electrochemical impedance spectroscopy, and electrochemical noise etc.

2.8.4.2.1 Potentiodynamic Testing:-

In potentiodynamic testing, current represents rate with which anodic & cathodic reaction taking place on the working electrode. In general cathodic current are considered to be negative & anodic current are considered to be positive. Typically current expressed in terms of current per unit area of the working electrode or current density [55]. These studies were carried out to obtain potential (with respect to SCE) v/s log of current density plot. This plot is commonly known as polarization curve. The potential range was selected in a manner so that sample could be polarized both ways i.e. cathodically and anodically.

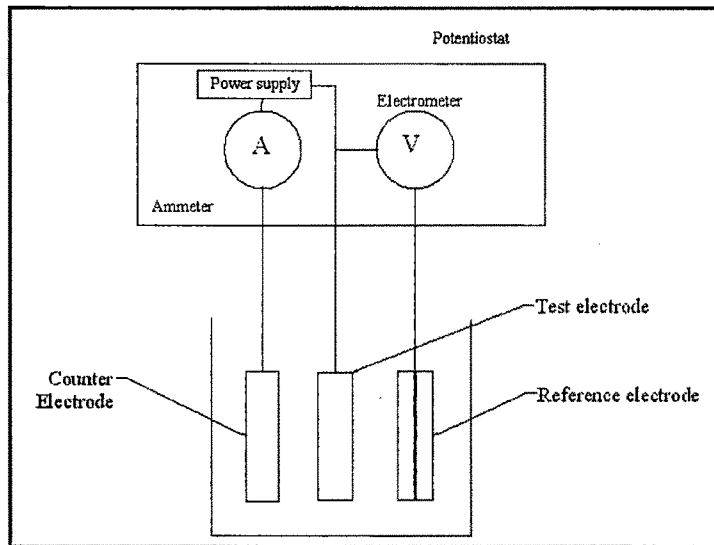


Fig 2.33 schematic diagram of Three electrode test cell

Fig.2.33 depicts a typical electrochemical corrosion test cell consisting of three electrodes

1. Working electrode (test specimen)
2. Counter or auxiliary electrode (Graphite electrode)
3. Reference electrode(calomel electrode)

A potentiostat is usually used for electrochemical measurements. It is generally connected to the three electrodes as shown in the Figure 2.33 above and then to a computer which has relevant software. The potentiostat when started automatically varies the potential at a steady rate between two preset potentials which generates current through the cell. The current supplied goes into the working electrode through the counter electrode which lead to dissolution of working electrode and shift potential from its equilibrium potential of that alloy called as polarization. This deviation of the potential of the working electrode could thereby be measured with respect to the reference electrode. Data logging of the potential and current could be done by the computer. [56, 57].

Potentiodynamic study is performed to determine

- Electrical double layer capacitance.
- Corrosion rates.
- Corrosion resistance.
- Organic coating capacitance and pure resistance.

2.8.4.2.1.1 Tafel extra proration method for Corrosion measurements:-

The Tafel plot corrosion measurement method uses a wide DC potential spectrum (400 to 500 mV) and provides more corrosion information than linear polarization. The Tafel plot has anodic and cathodic branches, corresponding to the anodic and cathodic half reactions for metal corrosion. Tafel plots can be classified as either activation or diffusion controlled. Tafel plots are classified as activation controlled when the corrosion rate is determined by how fast a metal is capable of transferring its electrons to electrolyte EAS. Tafel plots are classified as diffusion controlled when EAS diffusion rate determines the corrosion rate.

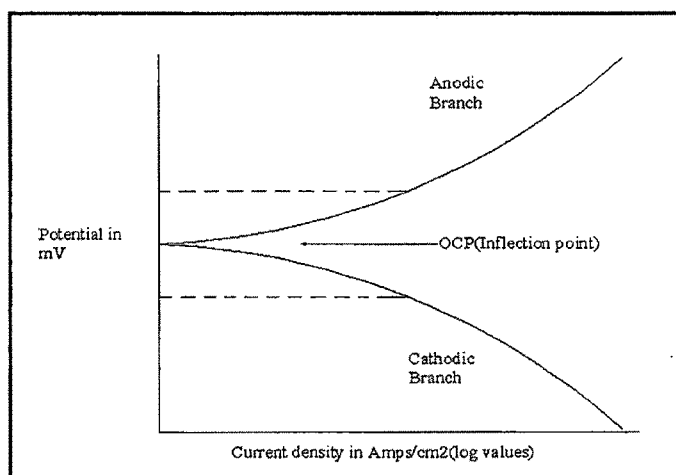


Fig. 2.34 Tafel plot for activation controlled corrosion rates.

Fig. 2.34 contains an example of a Tafel plot where corrosion reaction activation energy controls the corrosion rate. A characterization of activation control is increasing current density magnitudes with potential increases of both branches. Both branches become linear at some mV value from OCP this region is known as Tafel region. Fig.2.35 contains example of diffusion controlled Tafel Plots. Diffusion control theoretically causes cathodic current density to become constant at approximately -50 mV from OCP, as illustrated by the solid(ideal) plot. However, there are diffusion controlled plots whose current increases slightly with potential changes, as illustrated by the dashed plot. The slowly changing, cathodic current is referred to as the diffusion limited current, as noticed below:

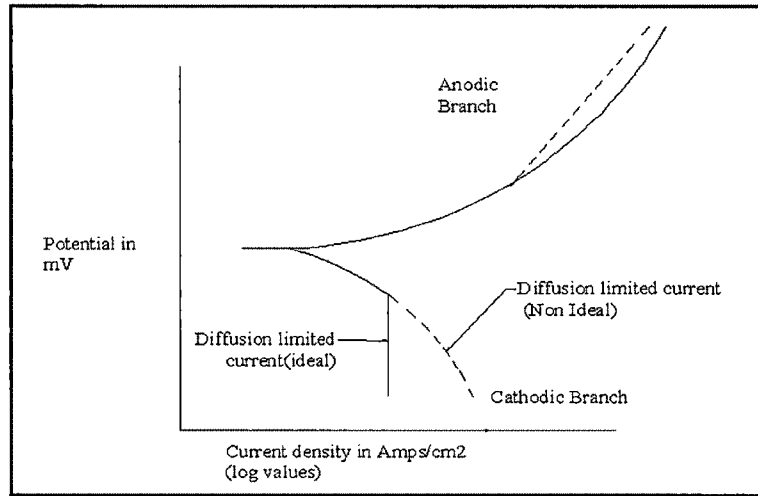


Fig. 2.35 Tafel plot for diffusion controlled corrosion rates.

2.8.4.2.1.1.1 Corrosion rates from Tafel slopes:-

Tafel slopes have units of volts per current-density-decade, where a decade is one order of magnitude current density, such as from 0.10 amp/cm²; Figure 2.36 illustrates how to estimate the cathodic slope (α_a & α_c), Tafel slopes can be used with linear polarization data when more accurate corrosion rates are desired.

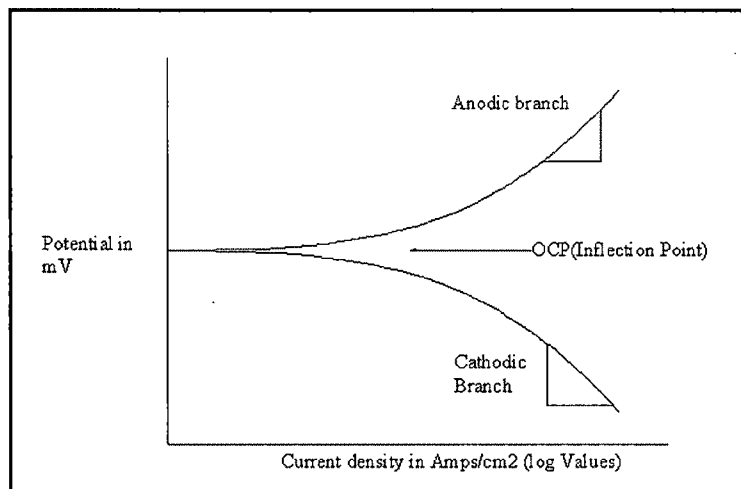


Fig.2.36 Determine Tafel Slopes from Tafel Plots.

Corrosion current is read directly from plot without the need for Tafel slope values or use of Stern and Geary equation ($i_{corr} = [1 / (2.303R_p)] [(\alpha_a \times \alpha_c) / (\alpha_a + \alpha_c)]$), fig. 2.37 & fig.2.38 illustrates how corrosion rates are obtained from both activation and diffusion controlled Tafel plots, respectively.

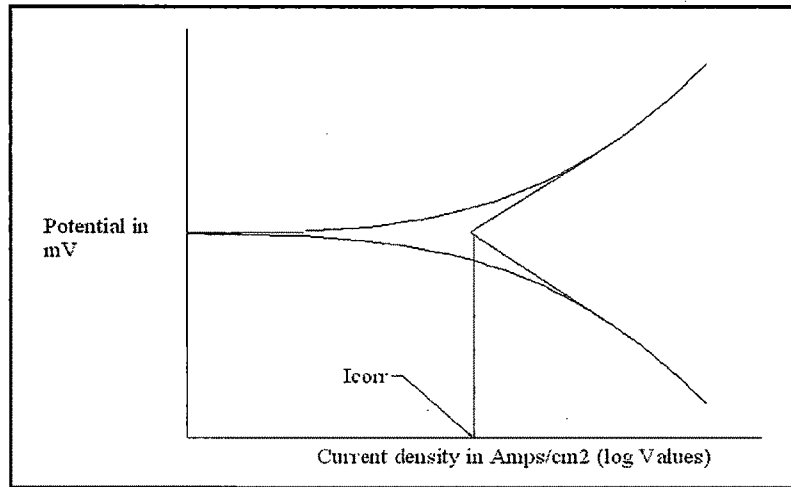


Fig. 2.37 Corrosion current flow activation controlled Tafel Plots.

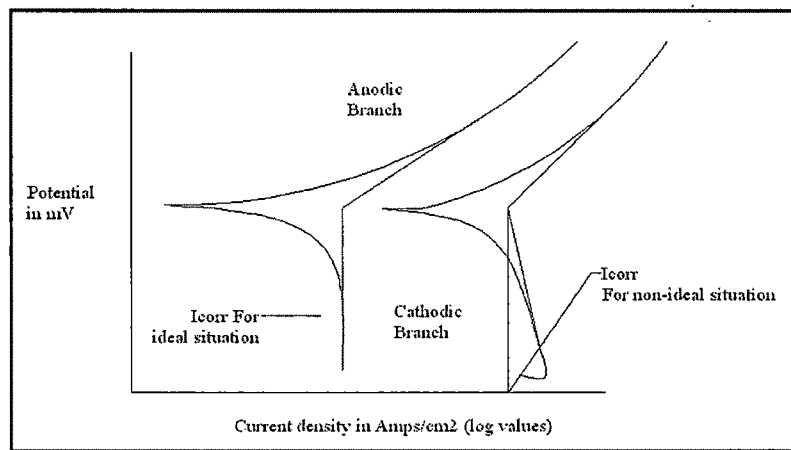


Fig. 2.38 Corrosion currents from different controlled Tafel plots.

Corrosion current for an activation controlled Tafel plots is the intersection of the anodic and cathodic linear extrapolation at OCP, as shown in fig.2.37. The corrosion current can be further converted to a corrosion rate in mils/year (mpy), using the following equation;

$$MPY = I_{corr} (\text{Å}) (1/\tilde{n}) (\tilde{a}) \text{ here,}$$

Å is combination of several conversion terms and is 1.2866×10^5 [equivalents*sec*mils]/[Coulombs*cm*years]

I_{corr} = corrosion current density in Amps/cm²

\tilde{n} = density of the metal in grams/cc.

\tilde{a} = equivalent weight in grams/equivalent.

Corrosion current is the diffusion limited current is constant with decreasing potential while in non-ideal diffusion controlled Tafel plot it is the intersection of linear extrapolations for both branches of OCP. It is important to remember that diffusion limited densities are a function of electrolyte stirring rate [58].

2.8.4.2.2 Cyclic polarization Testing

It is an electrochemical test method which is used to determine susceptibility to localized corrosion of the self passivating alloys in different corrosive environments. According to Silverman (1998; 2000), the technique is based on the idea that corrosion could be predicted by observing the response to a controlled upset from steady-state behavior; this may perhaps be created by application of voltage or current. Voltage could ramp in a cyclic manner from the corrosion potential and the characteristics of the current generated during the cycle are used to predict possible behavior at the corrosion potential. The voltage applied between a working electrode and the counter electrode could ramp at a continuous, slow rate relative to a reference electrode using a potentiostat. The voltage is increased in the anodic direction (forward scan) and could be reversed at some preset current or voltage. The potential at which the scan started is usually the corrosion potential measured when the corrosion process reaches steady-state. Breakdown potential for pitting, repassivation (protection) potential and hysteresis behavior (difference between forward and reverse anodic scans) data are acquired from the polarization curve which is used to compare the pitting corrosion resistance of test materials [59].

2.8.4.2.2.1 Purpose of cyclic polarization study are

- Study the pitting behavior of an alloy
- Determination of pitting potential
- Determination of corrosion potential
- Study the passivation behavior of alloy
- Study polarization (anodic & cathodic) behavior of alloy

2.8.4.2.2.2 Pitting and Repassivation Potentials

Two potentials that are often thought to characterize an alloy in terms of localized corrosion are the repassivation potential and the pitting potential and their values relative to the corrosion potential.

Pitting potential: The pitting potential is related qualitatively to the resistance of a material to a loss of passivity by pit initiation. It is potential at which a rapid rise in current during forward or ascending portion of the scan. The electrode surface exhibits small pits after the experiment.

Repassivation potential: It is potential at which damage passive film will repaired and decrease further pitting corrosion. There are several ways to choose the repassivation potential. It can be chosen as the potential at which the anodic forward and reverse scans cross each other. Alternatively, it can be chosen as that potential at which the current density reaches its lowest readable value on the reverse portion of the polarization scan. In case when forward and reverse portions of the polarization scan do not cross each other & loop does not close, then it can be estimated by extrapolating the reverse scan to zero current.

2.8.4.2.2.3 Cyclic polarization Scan Hysteresis loop

The hysteresis refers to a feature of the polarization scan in which the forward and reverse portions of the scan do not overlay each other. The hysteresis is the result of the disruption of the passivation chemistry of the surface by the increase in potential and reflects the ease with which that passivation is restored as the potential is decreased back toward the corrosion potential.

2.8.4.2.2.3.1 Type of Hysteresis loop

2.8.4.2.2.3.1.1 Positive hysteresis

It is caused by the polarization to more noble potentials making the surface more passive. In this case the reverse scan current density greater than forward scans current density & repassivation potential (E_{rp}) less than Corrosion Potential (E_{corr}) which indicate the greater disruption of surface passivity that causes pitting to be occur and corrosion rate will increase because the damage passive film will not repaired. This consion shown in fig. 2.39 as follows.

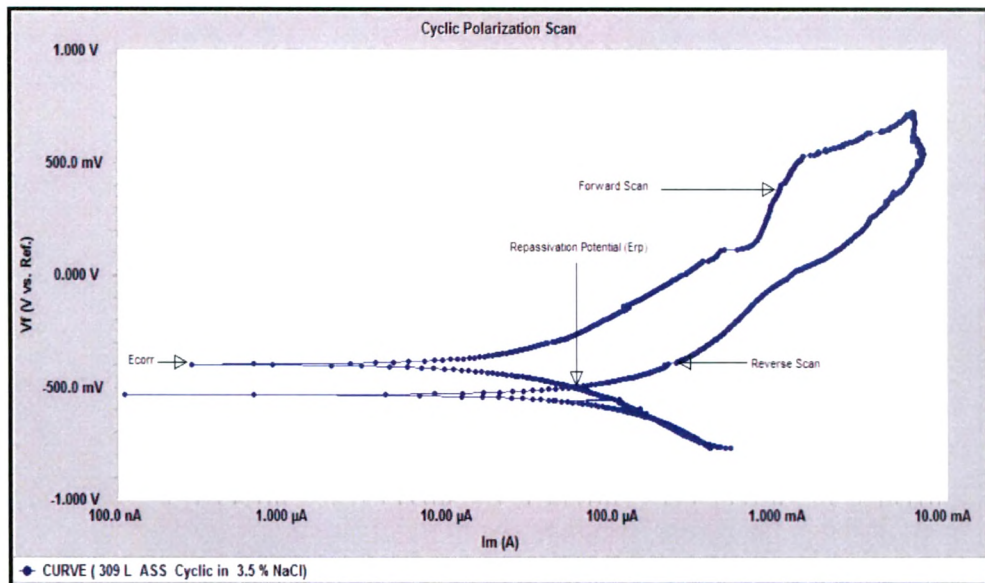


Fig.-2.39 Cyclic polarization scan with positive hysteresis

2.8.4.2.2.3.1.2 Negative hysteresis

It is caused by a decrease in passivity, often produced by the initiation of localized corrosion. In this case the reverse scan current density less than forward scans current density & repassivation potential (E_{rp}) greater than Corrosion Potential (E_{corr}) which indicate the less disruption of surface passivity as damage passive film will repaired causes decrease the pitting corrosion rate. This condition shown in fig. 2.40 as follows [60].

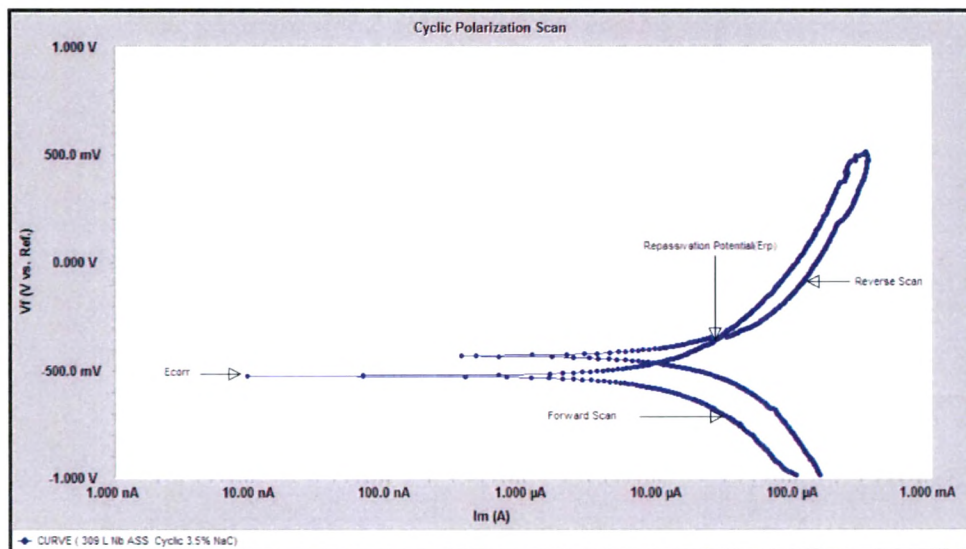


Fig.-2.40 Cyclic polarization scan with negative hysteresis

2.8.4.2.3 Inter Granular Corrosion Testing:

2.8.4.2.3.1 Electrochemical Potentiokinetic Reactivation (EPR) Test

ASTM A262 standard are used to determine the degree of sensitization of stainless steel A262-A practice, which consists of preparing a sample surface by polishing and then applying a corrosive attack with oxalic acid and observing the outcome with an optical microscope. The results are then classified into three categories (depending on the levels of precipitation): 'step', 'dual' or 'ditch', which refer to the standards established in ASTM A262. However, the techniques described in the latter are deficient in certain areas. They do not quantify the degree of sensitization and they are destructive in most applications. So to quantify degree of sensitization EPR methods developed.

2.8.4.2.3.1.1 Principle of Electrochemical Potentiokinetic Reactivation Test

Inter-granular attack is accelerated by potential differences between grain and grain boundaries, that is, attack is determined by availability of anodic sites at grain boundaries. Therefore, making it anodic passivated the specimen. At that time, the chromium depleted alloy sets up passive-active cell of appreciable potential difference, the grains (exhibit passive behavior) constituting large cathodic areas relative to small anode areas at grain boundaries (exhibit active behavior). During decreasing the potential, the protective passive film over Cr-depleted areas is more easily dissolved than that over un-depleted (non-sensitized) surfaces. The electrochemical potentiokinetic reactivation (EPR) test is based on the assumption that only sensitized grain boundaries become active, while grain bodies are un-sensitized. Thus, obtained curve of sensitized stainless steels will be different from the non-sensitized. This constitutes basis of EPR tests.

2.8.4.2.3.1.2 Single Loop Test Method

In the single loop test, a sample polished to a 1 micron finish, is polarized for two minutes at 200 mV vs SCE in a solution of 0.5M H₂SO₄ + 0.01M KSCN. Following this step, the potential is decreased at a rate of 6 V/hr to the corrosion potential, E_{corr}. This decrease results in reactivation of the specimen, involving breakdown of passive film covering chromium depleted regions of material. The area under the large loop generated in the curve of potential vs current, Figure 2.41 is proportional to electric charge, Q that depends on surface area and grain size. On non-sensitized material, passive film is intact and size of loop is small.

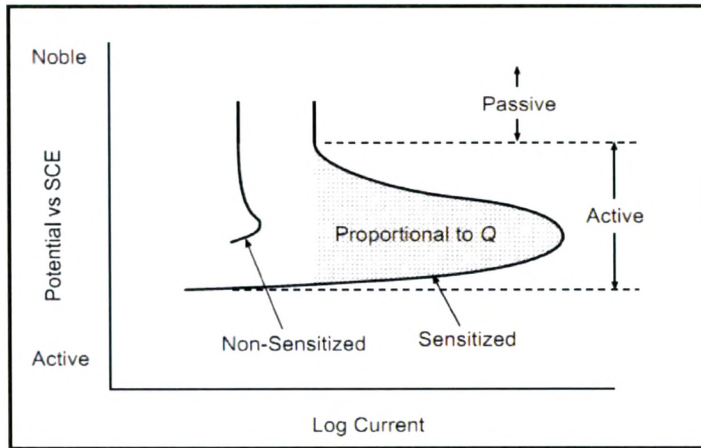


Fig. 2.41 Ideal Curve of Single Loop EPR Test Method

Then Q is normalized by total grain boundary area (GBA) as seen in equation below,

$$P_a = Q/GBA \text{ (C/cm}^2\text{)}$$

where, $GBA = A_s [5.09544 \times 10^{-3} \exp(0.34696X)]$, A_s is the specimen surface area and X is the ASTM grain size number. P_a can be selected as a tolerable level of sensitization for a given application [2]. Although this test has been standardized, there are major difficulties in using single loop EPR test, which are, the necessity of measuring grain size and polishing with 1 micron diamond paste, since reactivation behavior is very sensitive to surface finish. This led to the development of a new procedure that is the double loop test method, which basically sets a reference state of sample's own[61].

Interpretation of Single LOOP EPR study

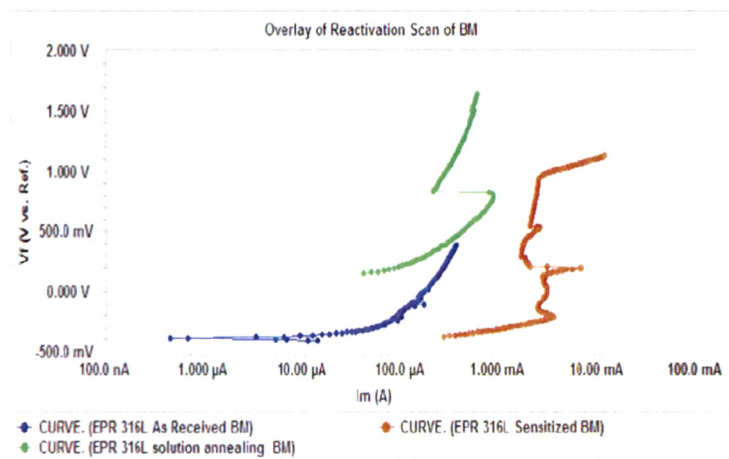


Fig. 2.42 Overlay of EPR test on 316 L Austenitic stainless steel welded joint.

Table-2.8 : Peak Current value of EPR test

| Peak Current Value (A/cm ²) | As Received | Sensitized | Solution Annealed |
|---|-------------|------------|-------------------|
| | 3.49E-04 | 1.12E-02 | 8.34E-04 |

Fig. 2.42 show the overlay of EPR test on 316 L Austenitic stainless steel welded joint. From the above table-2.8, It can be observed that samples which were subjected to sensitization treatments, the peak current values for sensitized sample was increased with respect to as received sample which indicate that that degree of sensitization were increased due to Cr_{23}C_6 precipitates at the grain boundary region. But after solution annealed, the peak current values was decreased as compared to sample which was subjected to sensitization treatments which indicate that degree of sensitization were due to dissolution of Cr_{23}C_6 precipitates in the matrix of austenite [62].

2.8.4.2.3.1.3 Double Loop Test Method

In this test, specimen is first polarized anodically through the active region then the reactivation scan in the reverse direction is carried out. When it is polarized anodically at a given rate from the corrosion potential to a potential in the passive area, this polarization leads to the formation of a passive layer on the whole surface. Then when scanning direction is reversed and the potential is decreased at the same rate to the corrosion potential, it leads to the breakdown of the passive film on chromium depleted areas. As can be seen in Figure 2.43, two loops are generated, an anodic loop and a reactivation loop. Evaluations of this method have shown that I_a is relatively insensitive to sensitization but I_r varies with degree of sensitization. I_r is small for unsensitized specimen whereas for sensitized specimen it increases. A ratio of maximum current generated in the double loop test ($I_r:I_a$) is used instead of area under reverse scan in single loop test and it is also not necessary to normalize the ratio of maximum current with the grain size. Moreover, in the double loop method, relatively rough 100-grit finish provides reliable data, which was not enough in the single loop method. In double loop method, since initially the specimen is activated anodically whole surface of the metal is lost, so surface is cleaned before reactivation scans. If this layer left in place, it covers sensitized

grain boundaries thus it can retard reactivation of these boundaries during the reactivation scan[61].

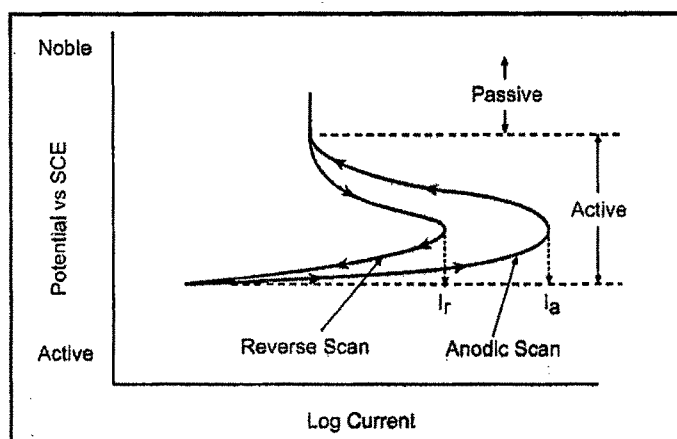


Fig. 2.43 Ideal Curve for Double Loop EPR Test Method

In the literature, there are many studies which deal with verification of EPR test method, comparison of double loop and single loop test methods and improving or applying test methods for different type of materials' susceptibility to intergranular corrosion. V. Cihal presented a study, which was a continuation of an earlier study dealing with electrochemical determination of sensitivity to intercrystalline corrosion of stainless steel, based on reactivation from passive state. He suggested that test method was verified on austenitic chrome nickel steels with increased carbon content and cold deformed. The ratio of charge during reactivation gave optimum quantitative criterion of tendency of steels to intercrystalline corrosion and intergranular stress corrosion. By changing experimental procedure, this method can be adjusted the other types of steels.

2.8.4.2.3.2 IGC Testing by ASTM A 262 Practice A to E

This specification covers the standard practices for detecting susceptibility to intergranular attack in austenitic stainless steels,

- These practices cover the following five tests:
 1. **Practice A—Oxalic Acid Etch Test**
 - Classification of Etch Structures of Austenitic Stainless Steels
 2. **Practice B—Ferric Sulfate–Sulfuric Acid Test**
 - Detecting Susceptibility to Intergranular Attack in Austenitic Stainless Steels
 3. **Practice C—Nitric Acid Test**

- Detecting Susceptibility to Intergranular Attack in Austenitic Stainless Steels

4. Practice E—Copper–Copper Sulfate–Sulfuric Acid Test

-Detecting Susceptibility to Intergranular Attack in Austenitic Stainless Steels

5. Practice F—Copper–Copper Sulfate–50 % Sulfuric Acid Test

-Detecting Susceptibility to Intergranular Attack in Molybdenum-Bearing Austenitic Stainless Steels

Table -2.9 : Applicability of ASTM standard practices in A 262 for testing of IGC in austenitic stainless steels

| Practice | Test | Temperature | Time | Applicability | Evaluation |
|----------|--|-------------|---------|--|---|
| A | Oxalic Acid Etch Screening Test | Ambient | 1.5 min | Chromium carbide sensitization only | Microscopic: classification of etch structure |
| B | Ferric Sulphate 50% Sulfuric Acid | Boiling | 120 h | Chromium carbide in 304, 304 L, 316,316L, 317, 317L, CF-3 & CF-8 Chromium carbide & sigma phase like constituent in 321, CF-3M & CF-8M is detected | Weight loss/corrosion rate |
| C | 65% Nitric Acid | Boiling | 240 h | Chromium carbide in 304, 304 L, CF-3 & CF-8 Chromium carbide & sigma phase in 316,316L,317, 317L,321,347, CF-3M & CF-8M End-gain in all grades | Weight loss/corrosion rate |
| D | 10% Nitric Acid 3% Hydrofluoric Acid | 70°C | 4 h | Chromium carbide in 316, 316 L, 317 & 317 L | Comparison of ratio of wt.loss of annealed sample to as-received sample |
| E | 6% Copper Sulphate 16% Sulfuric Acid Metallic Copper | Boiling | 24 h | Chromium carbide but sigma phase & end-grain corrosion is not detected. (All grade ASS) | Examination for fissures after bending |
| F | Copper Sulphate 50% Sulphuric Acid Metallic Copper | Boiling | 120 h | Chromium carbide in cast 316 and 316 L but sigma phase is not detected. | Weight loss/corrosion rate |

2.8.4.2.3.2.1 Practice A—Oxalic Acid Etch Test-

It will classified Etch Structures of Austenitic Stainless Steels. It is Rapid method of identifying specimens for susceptibility to IGA associated with $Cr_{23}C_6$ precipitates by simple etching. This practice is consider as screening test before the testing by Practice –B,C,D,E or F. as acceptable etch structures need not be subjected to the hot acid test but if the etch structures is non-acceptable, then there is need to be subjected to the hot acid test. It can be used to detect IGC tendency of extra low carbon grade &

stabilized grades 304L, 316 L, 317L, 321,347 are tested after sensitization heat-treatment at 650-675°C for 1 hr for maximum carbide precipitation.

Preparation of Test Specimen:

- Specimen size = 25 mm X 25 mm
- Grinded & polished up to 4/0 emery paper

Apparatus:

- DC power source: 15 V & 20 A
- Ammeter : 0-30 A
- Variable resistance:
- Cathode: a cylindrical piece of stainless steel
- Anode: specimen to be etch made anode
- Large electric clamp: to hold the test specimen
- Electrolyte : 10 % conc. Oxalic acid
- Etching condition: polished specimen etched at 1 A/cm² for 1.5 min.
- Metallurgical Microscope: For examination of etch structure

Classification of Etch Structure

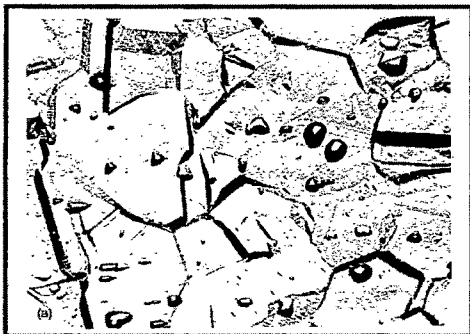


Fig.2.44 :Step Structure : (500X)



Fig.2.45 Dual Structure: (250X)

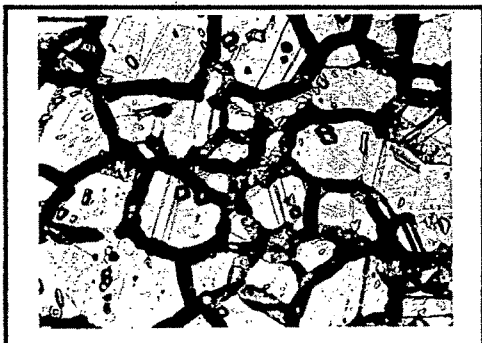


Fig.2.46 Ditch Structure (500X)

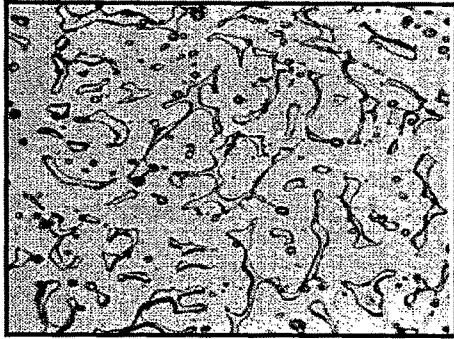


Fig.2.47 : Isolated Ferrite: (250X)

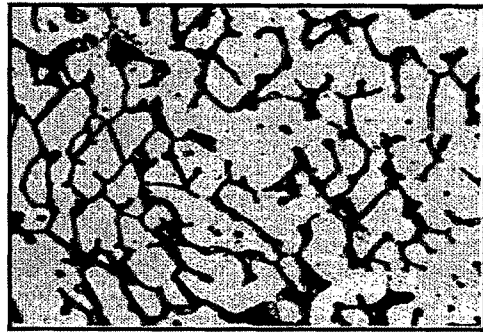


Fig.2.48 Inter-dendritic ditch: (250X)

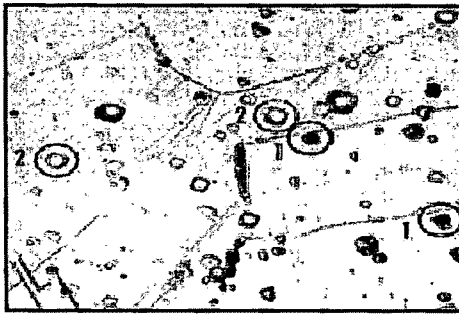


Fig.2.49 End grain pitting-I(500X)



Fig.2.50 End grain pitting-II(500X)

2.8.4.2.3.2.2 Practice B—Ferric Sulfate–Sulfuric Acid Test

It detect Susceptibility to Intergranular Attack in Austenitic Stainless Steels

Test Solution: Ferric Sulphate 50% Sulfuric Acid

Before this test, specimens may be given a rapid screening test in accordance with procedures given in Practice A. The Acceptable etch structure will be free from ICG may be subjected to practice – B but Non-acceptable etch structure need not to subjected to practice – B. The acceptable etch structure are step, dual, end grain I & II & isolated ferrite pools & non-acceptable etch structure are ditch & inter dendrites ditches.

Scope: It detects susceptibility to inter-granular attack associated with the precipitation of chromium carbides in un-stabilized austenitic stainless steels but does not detect susceptibility to inter-granular attack associated with sigma phase in wrought austenitic stainless steels containing molybdenum, such as Types 316, 316L, 317, and 317L but detect inter-granular corrosion associated with sigma phase in the cast stainless steels CF-3M and CF-8M. Specimens of extra low carbon and stabilized grades are tested after sensitizing heat treatments at 650 to 675°C (1200 to 1250°F), which is the range

of maximum carbide precipitation. The length of time of heating used for this sensitizing treatment determines the maximum permissible corrosion rate for such grades in the ferric sulfate–sulfuric acid test. The most commonly used sensitizing treatment is 1 h at 675°C (1250°F).

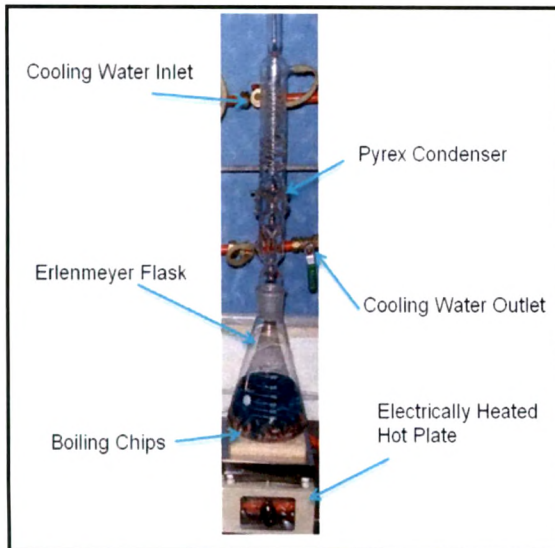


Fig.2.51 Apparatus of Practice B Test:

Fig. 2.51 shows the experimental set up for practice-B .Sample has been Continue immerse for the total 120 h without any interruption, then remove the specimen, rinse in water & acetone and dry.

2.8.4.2.3.2.3 Practice C—Nitric Acid Test (Huey Test)

(Detecting Susceptibility to Intergranular Attack in Austenitic Stainless Steels)

Test solution : 65± 0.2 weight % as nitric acid (Specific gravity 1.42)

Rapid Screening test: Before this test specimen is rapid screened tested by practice –A. The Acceptable etch structure will be free from ICG in practice – C but Non-acceptable etch structure need not to subjected to practice – C. The acceptable etch structure (CF-3, CF-8, 304, 304 L are Step, dual, end grain I & isolated ferrite pools & non-acceptable etch structure are ditch, end grain II & inter dendrites ditches

Scope: It is used to measure the relative susceptibility of austenitic stainless steels to intergranular attack. The presence or absence of intergranular attack in this test is not necessarily a measure of the performance of the material in other corrosive environments; in particular, it does not provide a basis for predicting resistance to forms

of corrosion other than intergranular, such as general corrosion, pitting, or stress-corrosion cracking. It is Huey Test which was first described by W.R.Huey in 1930. Reason of using this test Cr^{6+} ions is produced from the oxidation of Cr^{2+} and Cr^{3+} by HNO_3 , Cr^{6+} ions are accumulate in HNO_3 solution which increased the aggressiveness of environment. The boiling nitric acid test may be used to evaluate the heat treatment accorded "as-received" material. It is also sometimes used to check the effectiveness of stabilizing elements and of reductions in carbon content in preventing susceptibility to rapid intergranular attack. Intergranular attack in nitric acid is associated with (1) intergranular precipitation of chromium carbides, (2) sigma or transition phases in molybdenum-bearing grades, and (3) sigma phase constituents in stabilized grades. The boiling nitric acid test should not be used for extra-low-carbon molybdenum-bearing grades unless the material tested is to be used in nitric acid service. The most commonly used sensitizing treatment is 1 h at 675°C (1250°F). This practice may be applied to wrought products (including tubes), castings, and weld metal of the various grades of stainless steel.

2.8.4.2.3.2.4 Practice E—Copper—Copper Sulfate— 16 % Sulfuric Acid Test

Test Solution: Test solution will be contain 6 weight % of anhydrous CuSO_4 and 16 weight % H_2SO_4 (Specific gravity 1.84)

Copper Addition: Electrolytic grade copper shot or grinding may be used (shot is preferred for its ease handling before and after the test)

Rapid Screening test: Before this test specimen is rapid screened tested by practice -A. The Acceptable etch structure will be free from ICG in practice - E but Non-acceptable etch structure need not to subjected to practice -E.

Scope: It is conducted to determine the susceptibility of austenitic stainless steels to intergranular attack. The presence or absence of intergranular corrosion in this test is not necessarily a measure of the performance of the material in other corrosive media. The test does not provide a basis for predicting resistance to other forms of corrosion, such as general corrosion, pitting, or stress-corrosion cracking. This test indicates susceptibility to intergranular attack associated with the precipitation of chromium-rich carbides. It does not detect susceptibility associated with sigma phase. This test may be used to evaluate the heat treatment accorded as-received material. It may also be used to

evaluate the effectiveness of stabilizing element additions (Cb, Ti, and so forth) and reductions in carbon content to aid in resisting intergranular attack. All wrought products and weld material of austenitic stainless steels can be evaluated by this test.

Bend Test:

- The test specimen shall be bent through 180° and over diameter equal to the thickness of the specimen being bent.
- Bend axis shall be perpendicular to the direction of rolling.

Evaluation:

- Bent specimen shall be examine under low (5 X to 20 X) magnification
- The appearance of fissure or crack indicate the presence of Intergranular attack [63].

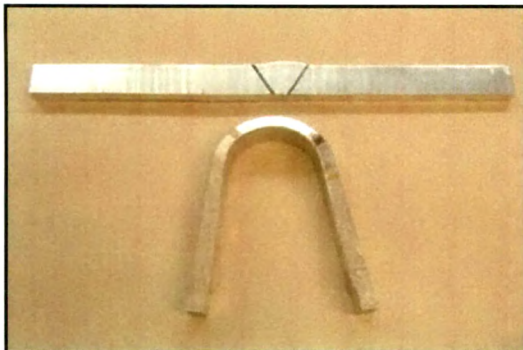


Fig. 2.52 Bend test after copper – copper sulfate 16 % sulfuric acid test



Fig.2.53 Passing Test Specimen (View the Bend Area 20X)

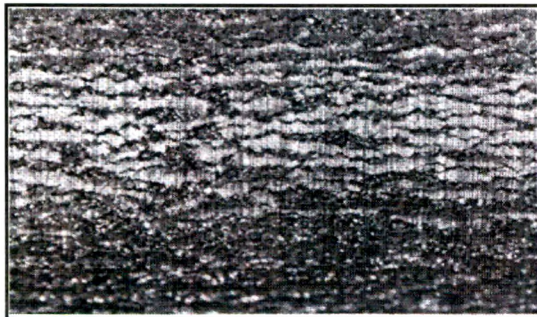


Fig.2.54 Falling Test Specimen—Many Intergranular Fissures (View the Bend Area 20X)

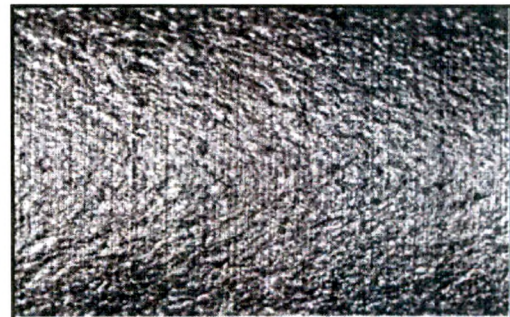


Fig.2.55 Doubtful Test Specimen—Traces of Intergranular Fissures & “orange-peel” surface (View the Bend Area 20X)

2.9 Problems & issues related to Electro-slag strip cladded weld-overlays

ESSC process is widely used in nuclear power plant, chemical & petro-chemical industry, offshore Industry, pulp & paper industry etc. to developed corrosion resistance & wear resistance weld overlay.

2.9.1 Hydrogen disbonding in weld overlays

Large pressure vessels are used in hydrogen containing environments, in the petroleum industry in hydro cracking, hydrodesulphurization and catalytic reforming processes, for example, and in the chemical and coal conversion industries. Many reactor vessels operate at high temperatures and at high hydrogen partial pressures. The vessels are generally fabricated from low alloy steel and need to be internally protected from high temperature corrosion. A protective layer is therefore frequently applied by weld surfacing. Typical specifications for the cladding are a chemical composition corresponding to AWS EQ347 (Nb- stabilized 18 per cent Cr 8 per cent Ni) with a ferrite content in the range of 3 to 8 or 10 per cent (or Ferrite Numbers). A 309LNb strip is frequently used for single layer solutions, whereas a 347 strip is used for the second layer and a 309L strip for the buffer layer in double-layer procedures[64].

2.9.1.1 Disbonding mechanisms

The operating conditions can vary significantly in hydrogen reactors, ranging from 200-600°C under hydrogen partial pressures of 1-60 MPa with 450°C and 15 MPa often being mentioned as typical values. During steady-state operating conditions in hydrogen reactors, there is a higher hydrogen concentration in the austenitic cladding than in the ferritic parent metal. When the reactor is cooled during shutdown, hydrogen attempts to diffuse from the steel. The lower solubility and higher diffusivity of hydrogen in the parent metal, compared with that in the austenitic cladding, leads to the build up of high hydrogen concentrations locally at the interface between the parent metal and the weld surfacing layer. Local over-saturation of hydrogen in combination with sensitive microstructures is known to cause hydrogen induced cracking (disbonding) in this region (Innterrante and Pressouyre, 1982). The exact mechanism of disbanding is under discussion, but it is thought to occur essentially as a result of hydrogen embrittlement. It is clear, however, that the resistance to disbonding is affected by the interface region

microstructure and is therefore dependent on the applied PWHT. Weld overlay disbonding has been observed, in some cases, during cool down of reactors. Crack propagation occurs in a narrow zone at the interface and along grain boundaries in the overlay close to the interface (Fig. 2.57).

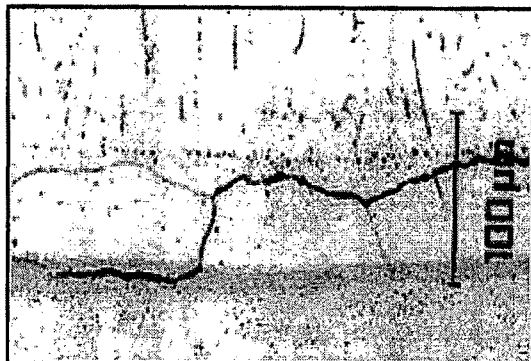


Figure 2.56 Disbonding in the interface region between parent material (bottom) and an austenitic overlay weld metal (top)

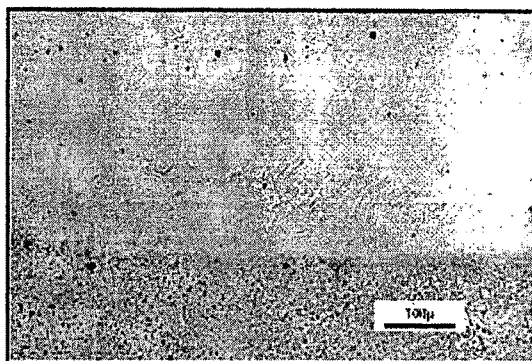


Figure 2.57 Martensite (light etching) in parent material / weld overlay interface region of an as-welded SAW overlay

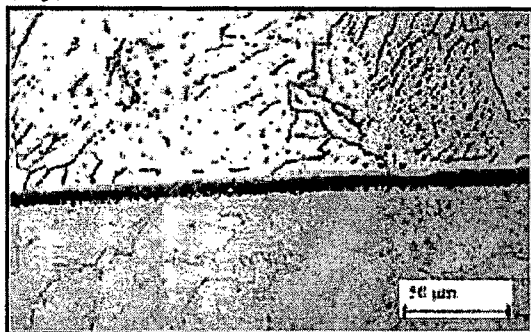


Figure 2.58 A comparatively narrow dark etching band of tempered martensite and carbides seen in an electroslag welded overlay after PWHT

Figures 2.56 – 2.58 gives some examples of interface region micro structures showing a band of tempered and/or untempered martensite and carbides typically found next to the interface. A ferrite-free region of typically 20 – 100 μm width separates the parent material from the normal ferrite-containing weld metal structure. A narrow band of martensite appears clearly in the weld overlay interface region in the as-welded condition (Fig. 2.57). The structure of the interface region for post weld heat treated welds consists

mainly of tempered martensite and carbides (Fig. 2.58). However, the higher hardness produced by a single PWHT as compared to double post weld heat treatment cycles suggests that fresh martensite can form during cooling from the PWHT temperature. Significant carbon migration is taking place during PWHT, as can be seen from the carbide precipitation and the formation of a 150 – 200 μm wide decarburised zone in the parent material (Fig. 2.58). The grain boundaries are also decorated by carbides in, and next to, the interface region[65,66].

2.9.1.2 Disbonding Test Methods

Several test methodologies exist for evaluating the susceptibility to hydrogen disbonding. Some of the important ones are described below:

2.9.1.2.1 Autoclave Testing

The most common method is by exposure of the test coupon in an autoclave at high temperature and high hydrogen pressure. The test temperature and hydrogen pressures are chosen with reference to the actual service conditions. Following exposure, the specimens are cooled to ambient temperature at a controlled rate. A cooling rate of 150°C / h is commonly used for qualification testing. The specimens are then held at room temperature for a designated period to allow for development of cracking between the stainless overlay and the steel. Following the hold period, the specimens are evaluated for disbonding by ultrasonic methods often combined with metallographic examinations. The size and distribution of the disbonded region(s) are then characterised (Figs. 2.59 and 2.60) according to Table 2.10.

Table - 2.10: Ranking of ultrasonic test results according to ASTM G 146-01

| Area ranking | Area disbonded (%) | Distribution ranking | Distribution |
|--------------|--------------------|----------------------|---------------------------------------|
| A | 5 | 1 | Isolated disbonded regions |
| B | 5-10 | 2 | Interlinking disbonded regions |
| C | 10-30 | 3 | Disbonding at weld pass overlaps |
| D | 30-50 | 4 | Disbonding at joint with side overlay |
| E | 50 and above | 5 | Other (to be described) |

Various specimen geometries are used but recent configurations utilize a round geometry, overlay on the top and side surfaces. The intention is to better simulate in-service behaviour with respect to hydrogen diffusion during cool down.

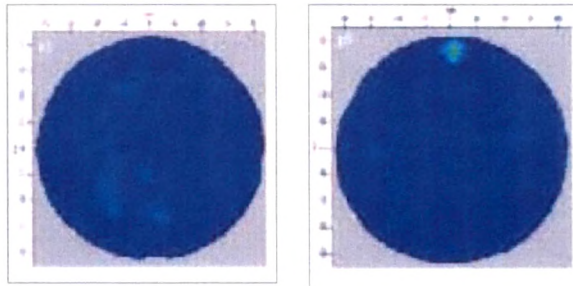


Figure 2.59 Ultrasonic top view scans showing the area of disbonding after testing. **Left: No disbonding. Right: With some disbonding. Classification A1 (5%, isolated disbonded areas)**

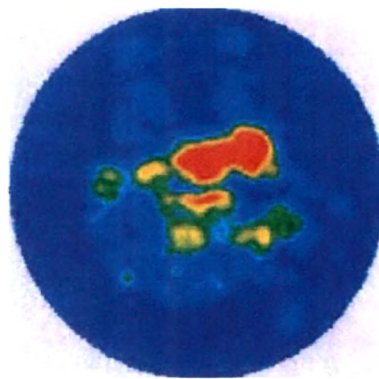


Figure 2.60 Ultrasonic scans showing significant disbonding. **Classification C2 with 10-30% interlinking disbonded regions according to ASTM G 146-01**

One-sided exposure an alternative test method corresponds to using the autoclave lid as the test sample. The autoclave lid is fabricated from the candidate overlay material system and placed on the autoclave clad side down. This method is, however, not widely used due to several limitations and disadvantages.

2.9.1.2.2 Cathodic charging:

Cathodic charging could, in principle, be an alternative test method. However, even though it is a rapid and easy technique, it has been shown to only distinguish between extreme cases. The method is, in practice, therefore, not used for purposes of overlay qualification.

2.9.1.3 Minimizing Disbonding Susceptibility:

Vessel wall material: As a first step, the base metal must be resistant to high temperature hydrogen attack, which can be ensured by selecting clean steels containing low levels of impurities (i.e. P, S and trace elements). A decreased carbon content also acts to reduce the amount of carbon diffusion into the overlay. The newer, vanadium modified Cr-Mo steels tend to have a lower susceptibility to hydrogen effects. This is claimed to be an effect of finely dispersed vanadium carbide precipitates trapping the atomic hydrogen. Consequently, there is a lower diffusivity of the hydrogen in the steel and the accumulation of hydrogen at the transition zone is lower compared to conventional Cr-Mo steels. Testing of double layer SAW and single layer ESW strip claddings of the 347 type, confirmed the excellent disbonding resistance of V-modified steels [66].

2.9.2 SCC Behavior of weld overlays:

Type 308 stainless steel was overlay by ESSC process as a internal cladding of reactor pressure vessels for boiling water reactors which is subject to post weld heat treatment (PWHT) during fabrication and can suffer sensitization depending on carbon and ferrite contents. This sensitization can be avoided by using niobium-added Type 308 weld metal (specified as Type 308 NbL) which was developed for one-layer overlay welding application. Stress corrosion cracking (SCC) behavior of heat-treated Types 308 and 308NbL weld metals in oxygenated high temperature pure water was evaluated by slow strain rate test and U-bend tests with and without crevice which showed that Type 308NbL weld metals were highly resistant to SCC compared to ordinary Type 308 weld metal as it were crack free over 23,000 hr. Using this analysis, the SCC life margin for Type 308NbL over ordinary Type 308 weld metals, expressed as a ratio of respective times to SCC initiation, was estimated to be about 36[67].

2.9.3 Effect of PWHT on Pitting Resistance of weld overlays:

Submerged arc welding (SAW) was employed to prepare the overlay weld of Type 347 SS over Type 309L SS plate is sometimes incorporated in the manufacture of petroleum hydro-desulfurization reactors made of 2.25Cr - 1Mo pressure vessel steel. It was subjected to post weld heat treatment (PWHT) at 690 °C for 8 hr .In the weld of austenitic stainless steel, at least 5%, by volume

of delta ferrite in the microstructure is required to minimize the thermal cracking during the weld solidification. On the other hand, Thomas has noted that the ductility of the weld is reduced when the δ ferrite content is higher than 10%. For austenitic SS weld, the relaxation of thermal residual stress and the improvement of ductility can be achieved by PWHT [68]. However, phase transformation or precipitation of carbides may occur in the meta-stable austenite/ferrite weld during PWHT process. One inter-metallic phase known as sigma phase can be transformed from delta ferrite when heat treated at elevated temperature.

Research by I-Hsuang Lo & Wen-Ta Tsai shows that in the as-welded Type 347 stainless steel overlay, delta ferrite and NbC were found in the austenitic matrix. Post weld heat treatment at 690°C for 8 h resulted in the additional formations of sigma phase and M_{23}C_6 . The presence of sigma phase resulting from eutectoid decomposition of delta ferrite caused an increase in the pitting corrosion susceptibility of Type 347 SS overlay weld. Multi-pass welding was applied. It is subjected to PWHT at $690 \pm 8^{\circ}\text{C}$ for 8 hr.

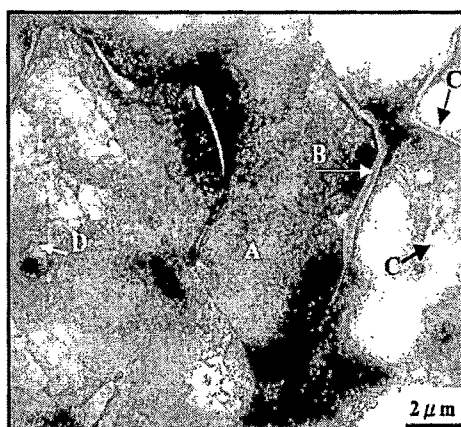


Fig. 2.61 A bright field image of welding overlay without PWHT.

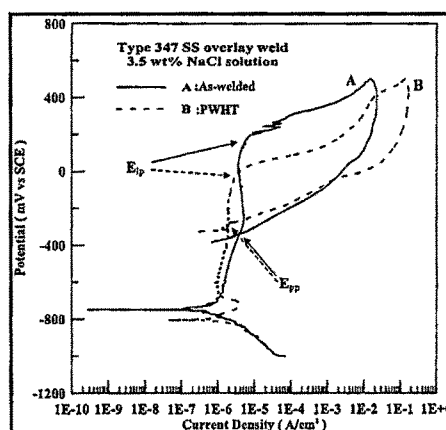


Fig. 2.62. Potentiodynamic polarization curves for Type 347 SS overlay welds, as-welded and with PWHT, in 3.5 wt.% NaCl

Fig. 2.61 shows primary phase ('A') is austenite & secondary phase marked as 'B'

is ferrite. The potentiodynamic polarization curves demonstrated that the overlay with PWHT had a higher susceptibility to pitting corrosion as compared with the as-welded. The density of pits on the as-welded overlay was lower than that on the PWHT after potentiodynamic polarization curve measurements. The potentiodynamic polarization curves of Type 347 SS overlays, with or without PWHT, are shown in Fig.2.62 Pitting initiation potential (E_{ip}) of the as-welded Type 347 SS overlay was 200 mV which is higher than that of the PWHT -300 mV indicating that the as-welded overlay was more resistant to pit initiation in 3.5 wt.% NaCl solution. The most susceptible corrosion site for Type 347 SS overlay (with PWHT) was found to be at the ferrite-austenite interface as revealed in the SEM micrograph (Fig.2.63). The presence of sigma phase, preferentially formed in the ferrite-austenite interface, was the main cause for the increase of pitting corrosion susceptibility.

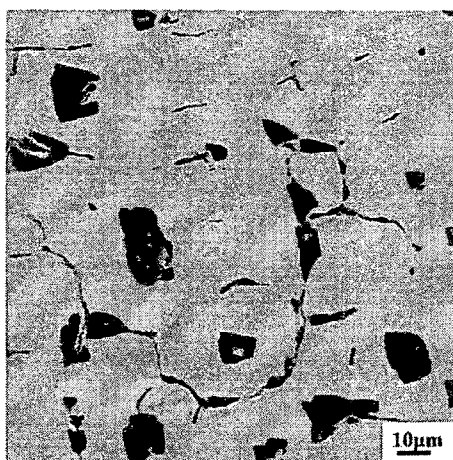


Fig. 2.63 Pits formed in the d/g interface of Type 347 SS overlay welds with PWHT after potentiodynamic polarization curve measurement in 3.5 wt.% NaCl solution.

Two different shapes of corrosion pits were found for the as-welded and the PWHT overlays, respectively, after potentiodynamic polarization tests. The cross section micrograph shown in Fig. 2.64 (a) revealed that a subsurface with near-hemispherical shape of pit was formed in the as-welded specimen while pits with irregular shapes were observed for the PWHT specimen Fig. 2.64(b). Undersurface penetration of the pit was also seen in Fig. 2.64(b). The pit depth

of the PWHT was larger than that of the as-welded, indicating a higher pit growth rate of the former. The precipitates, mainly sigma phase, formed in the PWHT overlay certainly assisted the initiation and growth behavior of pitting corrosion and affected the pit morphology[69].

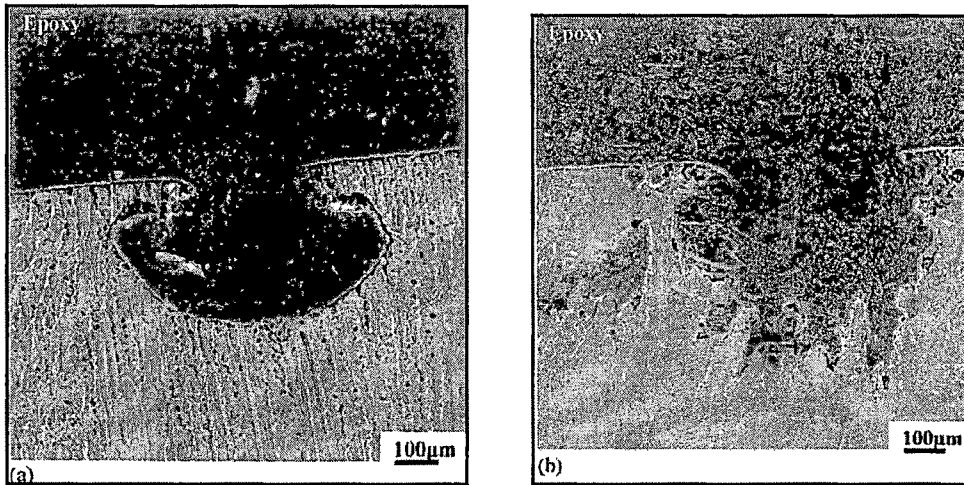


Fig. 2.64 SEM micrographs showing the cross-section morphologies of pits formed in (a) the as-welded, and (b) the PWHT Type 347 SS overlay welds after potentiodynamic polarization curve measurements in 3.5 wt.% NaCl solution.

2.9.4 Effect of PWHT on Inter-granular corrosion susceptibility of weld overlays :

Effect of carbon and ferrite contents on sensitization behaviour of stainless steel weld overlay have been discussed in several studies. Devine proposed a relation between the carbon content and the two-phase microstructure of ferrite-austenite (α - γ) for sensitization and rapid healing, which has succeeded in explaining mostly the behavior of two-phase Type 308 weld metals during PWHT. However, according to the I.Hamada & K.Yamauchi study, it was revealed that low-temperature aging (LTA) after PWHT could result in enhanced sensitization so-called low-temperature sensitization (LTS), even in healed weld metals. The LTS effect after PWHT thus found was supposed to be caused by the recurrence of chromium depletion around the chromium carbides (Cr_{23}C_6) on the α - γ grain boundaries. A possible way to suppress LTS after PWHT is to lower the carbon content to an extremely low level, and at the same time, to increase the number of α - γ grain boundaries as high as possible for a given amount of ferrite. However, by the

current welding technology, both the ultralow carbon weld metal as overlaid deposit, in which dilution of the low-alloy base metal is unavoidable, and the fine control of microstructure are practically impossible to realize in actual components. Another practical way to cope with these problems is to add a stabilizing element to a sufficient amount for sensitization resistance, considering any adverse effects on weldability and ductility. As a stabilizing element, niobium or titanium or both can be used.³ However, it is known that, in weld metals, titanium is rather difficult to maintain at the desired concentration because it can be consumed as nitrides or oxides during welding, and, hence, the resultant ability to stabilize the free carbon in the matrix during PWHT can be limited. This was demonstrated elsewhere for ferritic stainless steel weld metals. On the other hand, niobium-added weld metals, commercialized as Type 347 (UNS S34700), has been applied in chemical industries as an internal cladding of RPV[70]. I. Hamada & K. Yamauchi had studied the effect of Nb addition 308 austenitic stainless steel weld metal resistance to sensitization by post weld heat treatment (PWHT) at 600°C & Low temperature aging at 500°C for 24 hr after PWHT. In this work, 308 & 308 Nb austenitic stainless steel was applied as internal cladding of reactor pressure vessels for light water reactors by electro-slag welding process.

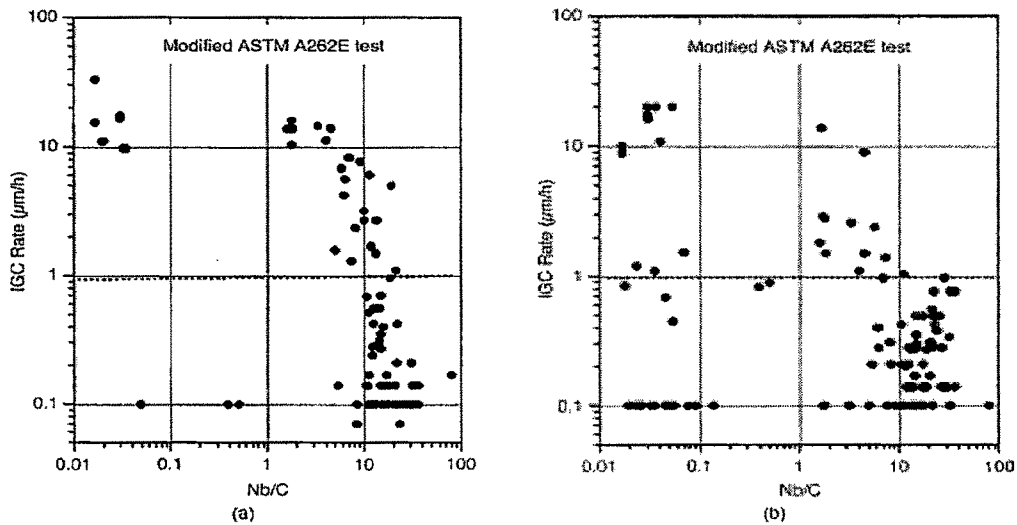


Fig. 2.65 Relation between Nb/C and IGC rate in two different heat treatments: (a) PWHT (6 h) + LTA and (b) PWHT (40 h or 50 h) + LTA.

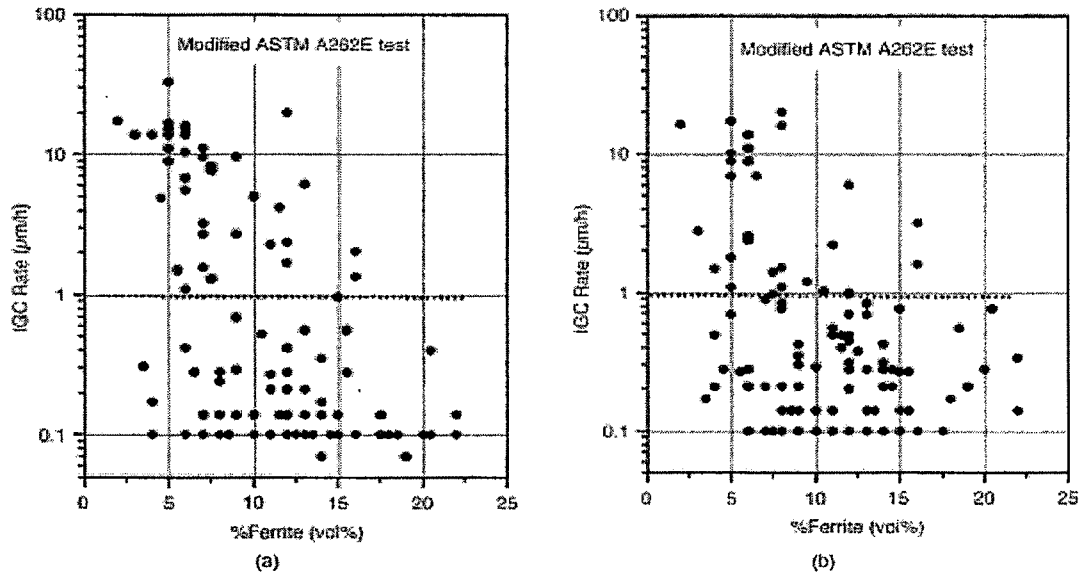


Fig. 2.66 Relation between %ferrite and IGC rate in two different heat treatments: (a) PWHT (6 h) + LTA (b) PWHT (40 h or 50 h) + LTA.

2.9.4.1 Effect of Nb/C on IGC Susceptibility

Figure 2.65 shows the effect of niobium addition on the IGC susceptibility of Type 308 weld metals as a function of Nb/C in the two metallurgical conditions. As is obvious from the results, the IGC susceptibility under PWHT (40 h or 50 h) + LTA became low when the Nb/C > 10. However, for the weld metals after PWHT (6 h) + LTA to satisfy the critical IGC rate ($\leq 1 \mu\text{m/h}$), the necessary ratio of Nb/C seemed to be much higher than 10. The observed difference in sensitization behavior with the two PWHT was thought to have come from the healing at longer PWHT. In other words, to achieve full stabilization in a certain range of PWHT, more niobium may be necessary if the effects of other factors (microstructures, etc.) are insignificant. In Figure 2.66, the IGC rates are plotted against ferrite content. Apparently, there was no significant relation between the two. Many data points fell into the IGC-susceptible region even though the amount of ferrite was >10 FN.

2.9.4.2 Reheat Embrittlement

The results of the bending tests are plotted against carbon and niobium contents in fig.2.67. The ferrite content of each sample are indicated with each symbol. The solid symbols denote that cracks were observed upon bending.

Based on the results shown above, it would be reasonable to attribute the fixation of carbon by niobium to the excellent resistance to IGC. However, it is not yet known in what way niobium stabilizes carbon in a two-phase microstructure. To examine this material issue, electron microscopy was used.

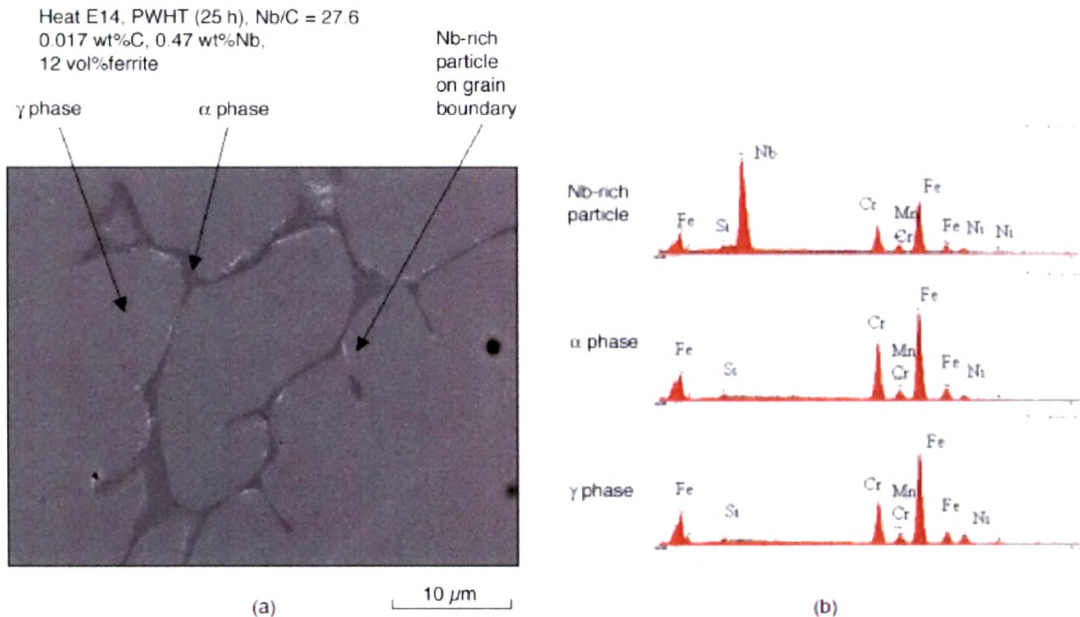


Fig. 2.68. (a) BSE image and (b) EDX analysis of mirror-polished Type 308NbL weld metal. Whitish particles rich in niobium are seen not only at α - γ grain boundaries but also in their vicinities.

Figure 2.68(a) is a back-scattered electron (BSE) image of mirror-polished Type 308NbL weld metal which was post weld heat treated at 600°C/ 25 h + 500°C/24 hr. Here carbon and ferrite contents were 0.017 wt% and 12 FN, respectively. According to Figure 2.68(b), the phases, observed by BSE and analyzed by energy-dispersive x-ray analysis (EDX), were α , γ , and niobium-rich precipitates along the α - γ grain boundaries & some of the precipitates are seen in the γ phase in the vicinity of the α - γ grain boundary.

The result show that a typical one-layer Type 308NbL to be immune to sensitization and reheat embrittlement in a wider range of heat treatments including the LTA effect because weld metals was found to be generally finer than that of ordinary Type 308 weld metals in terms of a distribution of α phase, or the number of α - γ grain boundaries & NbC, prior to

Cr_{23}C_6 , would precipitate preferably along α - γ grain boundaries and reduce the carbon level in the matrix significantly [71].

2.9.5 Effect of Ferrite content on Inter-granular corrosion susceptibility of weld overlays

In nuclear industry, strip welding with submerged arc or electroslag technique was most common techniques for production of RPV clad, and the microstructure of the clad was composed of a main part of fcc austenite, a few percent bcc δ -ferrite that was produced during overlay welding. Small amount of δ -ferrite is desirable in the weld zones of austenitic stainless steels, because the ferrite phase prevents hot tearing or cracking. On the other hand, the δ -ferrite could cause the thermal aging embrittlement through the decomposition of δ -ferrite to brittle sigma phase, and chromium rich carbide (M_{23}C_6 type), when it is exposed to the temperature range between 600 and 900 °C [72]. Previous research shows Nb is stabilize the carbon present in the steel, but the Nb content in > 0.95 % promoting the formation of sigma along with the other constituents such as Cr, Mo and Si after PWHT which mainly lowers the toughness and can lead to inter-granular corrosion.

2.9.6 Effect of welding speed on corrosion susceptibility of weld overlays

Micro-structural characteristics the different amount of sigma phase Cr_{23}C_6 & FeC, NbC precipitation between the clad is considered to be due to the different cooling rate resulted from the different heat input rates during overlay welding. The chemical composition and microstructure in the transition region of the interface between the overlay and the base steel depend heavily on the welding procedures, especially the welding speed. The welding speed has a considerable influence on bead geometry, ferrite content and dilution. If a very low travel speed is used with over alloyed strip during cladding of the first layer, the result would be a very low dilution but at the same time acquiring an unacceptable high content of ferrite & coarse grain structure of weld metals and especially the precipitations of inter-metallic phases such as sigma phase, Cr_{23}C_6 .

A high speed welding procedure would produce an overlay with faster cooling rates in the fusion region, resulting in a finer grain structure and the inhibition of the formation of planar grain boundaries. Also, the finer grain structure would reduce the concentration of

impurities on grain boundaries. On the other hand, the grain growth in the base metal side would be retarded due to the faster thermal cycle of high speed heating and cooling[73]. So, welding with higher speed is not only an economical factor but also a metallurgical one. With strip electrodes of 60x0,5 mm for electroslag cladding, welding speeds of 18 to 20 cm/min are selected as usual parameters (about 1,200 Amps and 24 Volts). If the requested thickness of the overlay is more than 5 mm, a second layer with another strip is recommended instead of cladding a single thick layer with high ferrite content[74].

2.9.7 Effect of PWHT & Heat input on Inter-granular corrosion susceptibility of weld overlays:

Researchers J.S. Lee , I.S. Kim , R. Kasada & A. Kimura had investigate the effect of microstructure of the clad that depends on the heat input rate during submerged arc welding process to developed cladded with 309 L grade austenitic stainless steels on the inner wall of nuclear reactor pressure vessel(RPV).Heat treatment conditions during overlay welding and post weld heat treatment as follows:

Preheating: 121⁰Cmin.

Inter-pass heating :176⁰Cmax.

Posting heating: 210–310 ⁰C/2 h

Postweld heat treatment (PWHT): 620–628 ⁰C/41 h

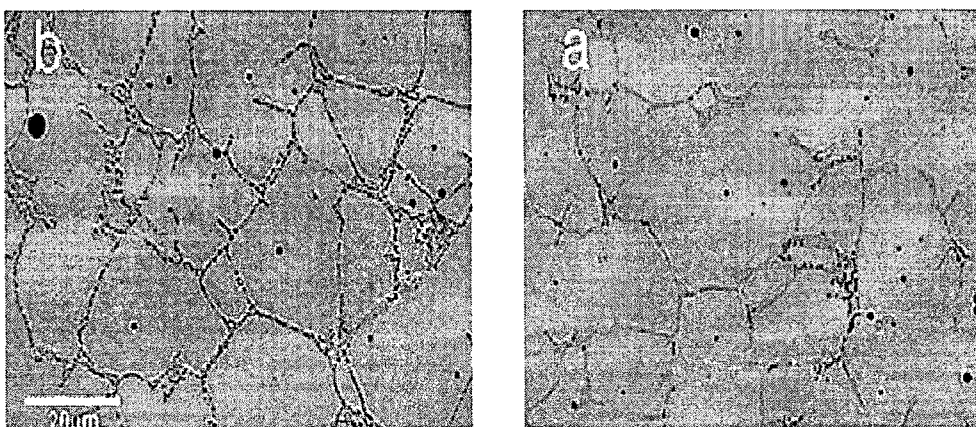


Fig. 2.69 Scanning electron micrographs of RPV clad, gray= γ austenite, dark gray= δ ferrite plus σ phase, backscattered electron (BSE) mode: (a) K001, (b) K002J.

Table 2.11: The maximum heat input rate and volumetric phase fractions (%) of RPV clad

| Index | Max. heat input rate(kJ/cm) | δ -Ferrite (FN) before PWHT | δ -Ferrite (FN) after PWHT | σ -phase |
|-------|-----------------------------|------------------------------------|-----------------------------------|-----------------|
| K001 | 164.4 | 9.1 | 6.6 | 1.9 |
| K002J | 188.5 | 10.2 | 2.5 | 7.9 |

Fig. 2.69 presents typical microstructure of 309L clad varying with the heat input rate during submerged arc welding, indicating that both the clads were composed of about 90% fcc austenite, a few percent of bcc δ -ferrite and brittle σ phase. The δ -ferrite was mainly formed at the austenite grain boundaries. As listed in Table 2.11, the higher heat input prior to PWHT (K002J sample) resulted in a slightly larger fraction of δ -ferrite than the lower one (K001 sample) [75].

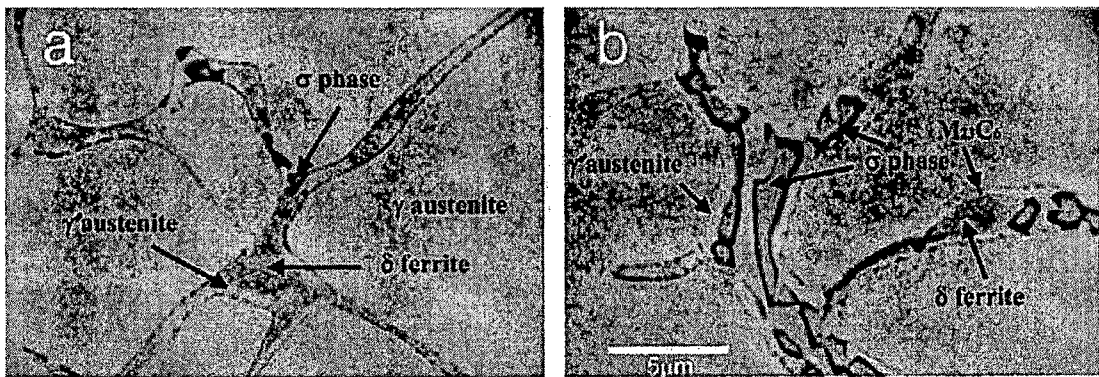


Fig. 2.70. Typical microstructural characteristics of inside of δ -ferrite, gray= γ austenite, white gray= new austenite (γ'), dark gray= δ -ferrite, black= σ phase, backscattered electron (BSE) mode: (a) K001, (b) K002J.

Fig. 2.70 shows the micro-structural features of the clads, especially inside of δ -ferrite after applying the PWHT. Since we used a backscattered electron (BSE) detector for SEM observation, σ phase, which contained high percentage of chromium, represented as dark color compared to the δ -ferrite and γ austenite. Images produced by BSE show characteristic atomic number contrast, that is, features of high atomic number (Z) appear brighter than those of low Z . In K002J clad, the initial ferrite-austenite boundaries moved into the δ ferrite and the remaining was almost transformed to γ and new austenite (γ') during PWHT. In the mean time the formation of σ in K001 clad was not significant,

Since K002J sample was fabricated with high heat input rate, it might result in a slower cooling rate than that of K001 sample. It was reported that if cooling rate was decreased, the volume fraction of sigma phase precipitation was increased & also another possibility is the difference of total available chromium atoms in delta ferrite phase consumed to form a sigma phase during PWHT [76]. Since the chromium is the stabilizer of ferrite phase, the delta ferrite can possess higher chromium compared with the austenite phase.

Further, before PWHT the volume fraction of delta-ferrite in K002J clad were larger than those in K001, the total amount of available chromium in K002J clad was larger than K001. Accordingly, K002J clad had a higher potential to form the σ phase, and resulted in the larger fraction of r in K002J clad rather than in K001 (Table 2.11). The PWHT on the clad resulted in a reduction of d-ferrite content and that is interpreted in terms of the decomposition of d-ferrite to new austenite (γ'), chromium rich carbide ($M_{23}C_6$ type) and sigma phase during the heat treatment. The decomposition of delta-ferrite during PWHT may proceed through the precipitation of chromium rich carbides occur at initial ferrite – austenite boundaries by the eutectoid reaction ($\delta = M_{23}C_6 + \gamma'$) and evoked the movement of ferrite-austenite boundaries into the delta-ferrite. Then, the formation of sigma phase and new austenite (γ') by ($\delta = \sigma + \gamma'$) occurs. The sigma phase is a hard intermetallic phase with a complex tetragonal structure, which often causes the degradation of mechanical properties. It can be seen from this research that the microstructure of the clad was composed of a main portion of fcc austenite and a few percent of bcc d-ferrite, and the transformation of d-ferrite during post weld heat treatment resulted in the formation of $M_{23}C_6$ type carbides at the initial δ/γ grain boundaries and brittle σ phase [77,78].

2.10 Origin of the Research Problem :

Large pressure vessels are used in hydrogen containing environments, for example, in the petroleum industry in hydro-cracking, hydrodesulphurization and catalytic reforming processes as well as in the chemical and coal conversion industries. All hydro processing reactors require internal protection of the reactor vessel walls experience electrochemical corrosion such as pitting corrosion, inter-granular corrosion, stress corrosion cracking & hydrogen disbonding. The most productive system for surfacing the large components

which are subjected to corrosion or wear is submerged arc strip cladding which is most frequently used but, if higher productivity and restricted dilution rates are required, electro-slag welding (ESW) is recommended. This protection is generally provided by stainless steel strip electrodes which are made up of different grade such as 304, 304 L, 347, 309L, 309LNb, 316L, 317L. Base on the literature review it was found that to increases the resistance against general corrosion & IGC susceptibility 309L austenitic stainless steel strip has been used. Addition on niobium in 309L will improve the general corrosion, IGC susceptibility as well as pitting resistance. During ESSC process it was found that The welding speed has a considerable influence on bead geometry, ferrite content and dilution & Micro-structural changed of the weld overlay as If welding speed is low would be a very low dilution but at the same time acquiring an unacceptable high content of ferrite & coarse grain structure which lead to increase the susceptibility toward IGC while higher welding speed would produce an overlay with faster cooling rates in the fusion region that resulting in a finer grain structure and the inhibition of the formation of planar grain boundaries and hence decrease susceptibility toward IGC. During cladding process base metal experience high amount of solidification stresses which can be relieved by subjecting it to PWHT at 690⁰C for prolong period of time but at same this may increase the susceptibility toward IGC & pitting corrosion of weld overlay due to formation inter-metallic precipitation such as of Cr₂₃C₆ & sigma phase which is very essential to understand.

2.10.1 Scope of Work:

Base on this review, it was decided that two different grade of austenitic stainless steel 309 L & 309 L Nb were selected to developed weld overlay on low carbon low alloy steel (Cr-Mo Steel) by varying welding speed from 160 mm/min to 200 mm /min at fixed current and voltage ranges. Weld overlay also subjected to post weld heat treatment PWHT at 690⁰C for 24 hour of time to relive thermal stresses which are generating during welding process. Weld overlay are under gone various corrosion problems such as general, pitting and inter granular corrosion under service conditions & micro structural changes, hardness & mainly pitting & inter granular corrosion after PWHT. So the corrosion behaviour of both weld overlay will be studied in different corrosive environments using various corrosion test such as potentiodynamic study, cyclic

polarization study, EPR test while micro-structural change were studied by optical microscopy & SEM .

2.11 Objectives of the Research Works:

1. Development of single layer weld overlay of 309 L & 3091 Nb grade austenitic stainless steel on Cr-Mo steel by ESSC process.
2. To study the effect of alloy variation at different location of the weld overlay in various corrosive environments.
3. To study the effect of welding parameters on corrosion resistance, microstructure & mechanical properties of weld overlay.
4. To study the effect of niobium addition on corrosion resistance, microstructure & mechanical properties of weld overlay.
5. To study the effect of post weld heat treatment (PWHT) on corrosion resistance, microstructure & mechanical properties of weld overlay.